The effect of out-of-plane constraint on the stress fields near the front of a crack in a thin ductile plate

D.K. Yi , T.C. Wang

PII: S0020-7683(19)30431-7
DOI: https://doi.org/10.1016/j.ijsolstr.2019.10.008
Reference: SAS 10508

To appear in: *International Journal of Solids and Structures*

Received date: 5 June 2019
Revised date: 14 September 2019
Accepted date: 6 October 2019

Please cite this article as: D.K. Yi , T.C. Wang , The effect of out-of-plane constraint on the stress fields near the front of a crack in a thin ductile plate, *International Journal of Solids and Structures* (2019), doi: https://doi.org/10.1016/j.ijsolstr.2019.10.008

The effect of out-of-plane constraint on the stress fields near the front of a crack in a thin ductile plate

D.K., Yi[a,*], T.C.,Wang[b]

[a] College of Mechanics and Materials,

Hohai University, China

[b] LNM, Institute of Mechanics,

Chinese Academy of Science, China

Abstract

Classical plane solutions based on the elastic-plastic fracture mechanics are applied widely in practical engineering. These plane solutions follow the plane stress or plane strain assumption. However, in the case of a thin ductile plate with a through-thickness crack under tension, plane stress conditions exist at a distance of about one half of the plate thickness ahead of the crack front cross the thickness of the plate. What is the stress state in the region where both plane strain and plane stress conditions cannot be met? In the current paper, a semi-analytical method is presented to investigate the problem. Three dimensional Maxwell stress functions, the minimum complementary potential energy principle and three dimensional *J*-integrals are employed to obtain solutions for crack front fields in a thin ductile plate. Three-dimensional finite element (FE) analyses are carried out to verify the current solutions. FE results reveal that the out-of-plane constraint level T_z increases with increasing remote loading near the crack front. FE results also show that the in-plane stress fields near the crack front can be characterized by the current J-T_z solutions. Both FE and theoretical results illustrate that opening stresses decrease gradually to

the corresponding plane stress HRR-field solutions with increasing radial distance *r* from the crack front in the mid-plane when remote loading is large enough.

Key words: Elastic-plastic fracture mechanics; Three-dimensional singularity field; Out-of-plane constraint; Three-dimensional FM simulation

1 Introduction

In the past 50 years, a considerable amount of papers on two-dimensional analyses of cracked plate elements have been published (Williams, 1957; Dugdale, 1960; Irwin, 1961; Burdekin and Stone, 1966; Rice and Rosengren, 1968; Hutchinson, 1968; Rice,1968; Ritchie, et al., 1973; Shih, 1981; Rice, 1988; Betegon and Hancock,1991; O'Dowd and Shih, 1992, Hutchinson and Suo, 1992, Xia et al., 1993; Hill et al., 1996; Conner et al., 2003; Marsavina and Sadowski, 2007; Zhou and Wei, 2014, 2015; Ambati et al., 2015). Compared with corresponding three-dimensional analyses, two-dimensional analyses can be applied much more easily in practical problems. However, some theoretical analyses and experimental examples (Pook, 2013; He et al., 2016; Yi and Wang, 2018) have shown that the effect of three-dimensional constraint cannot be disregarded. Three-dimensional fracture analyses are without doubt needed for further comprehension of fracture behavior of plate elements.

In the 1970s, some attempts were made to solve three-dimensional elastic fracture problems. Hartranft and Sih (1970) and Sih (1971) presented an analytical approach to investigate the distribution of stress intensity factor along the front of a

crack in a thin elastic plate under uniaxial tension. Benthem (1977) presented an analysis solution for the singularity at the vertex of a quarter-infinite crack in an elastic half-space. Benthem's solutions showed that the vertex singularity depends on Poisson's ratios and is weaker than the square root singularity. Bazant and Estenssoro (1979) presented numerical results for the three-dimensional singular stress fields near the terminal point of an inclined crack front edge at the surface of an elastic body. These numerical results confirmed that vertex singularities exist and are weaker than the square root singularity. Yang and Freud (1985) studied the state of stress in a thin elastic plate which contains a through-thickness crack and derived a crack tip boundary layer solution for mode I loading. The solution showed there is a finite lateral contraction at the crack tip and the out-of-plane displacement on the free surface merges smoothly with the corresponding plane stress solution at distances from the tip of one-half to three-fourths of the plate thickness. Nakamura and Parks (1988) investigated the three-dimensional stress fields near the front of a crack in a thin elastic plate under tension using finite element methods. Numerical results presented by these authors verified Benthem's solutions for vertex singularities and revealed that stress intensity factors decrease sharply in the region near the free surface. The phenomena was explained later by Leung and Su (1996). Kwon and Sun (2000) presented a *K*-*V* model that the crack-front stress fields near the free surface of a cracked elastic plate under tension can be expressed as the superposition of *K*-field solutions and vertex-singularity-field solutions. In the new century, three-dimensional elastic crack problems were instigated further by many researchers. Kotousov (2004,

2007, 2010) presented a series of solutions for elastic plates of arbitrary thickness with a crack or a notch under tension or shear loading using the distributed dislocation technique. In the case of tension, the author concluded that the magnitude of stress intensity factor increases with increasing ratio of crack size to plate thickness. In the case of shear, the author revealed the plate thickness has a minor influence on the value of stress intensity factor but the intensity of the coupled K_O–mode (out-of-plane mode) increases with an increase of the plate thickness. Considering a crack in a plate made of a cubic single crystal under in-plane loading, Chaudhuri (2010) investigated the effect of crystal structure on the deviation of crack. The author believed that crack deviation will not appear if the single crystals under tension have a rock salt structure, however if the single crystals under tension have a bcc structure, crack deflection always happens. Nagai et al. (2012) presented a numerical method called M_1-integral method to evaluate the stress intensity factors along the front of an interface crack between dissimilar anisotropic materials subjected to thermal and mechanical stresses. Branco et al. (2012) investigated effects of geometrical parameters and material properties on the out-of-plane constraint level for three cracked geometries under two loading patterns. These authors revealed that the out-of-plane constraint level decreases slightly in an interior region, declines quickly in a near surface region and drops abruptly in a surface region when approaching the free surface. Similar results also can be found in Fig. 5 in the current paper. Kotousov et al. (2013) investigated coupled fracture modes in an elastic plate containing a through-thickness crack under shear or anti-plane loading using three-dimensional finite element methods. These

authors believed that shear or anti-plane loading can induce an anti-plane or shear singular stress fields near the crack front and the intensity of the coupled mode is affected strongly by the thickness of plate. Goes et al. (2014) examined 3D effects on the stress and strain fields near the tips of a notch and a long/short crack using finite element methods. They revealed that for a long crack, the three-dimensional zone ahead of the crack tip is up to 0.4 times the plate thickness, while for a short crack, the three-dimensional zone is up to 10 times the crack length. He et al. (2016) gave a brief review of recent studies on three-dimensional brittle fracture, especially the studies of coupled fracture modes and vertex singularities. Soliman et al. (2018) presented a new analytical generalization of *J* and *G*-theta integrals for planar cracks in a three-dimensional medium.

Three-dimensional analyses of ductile fracture are more complicated than the corresponding elastic analyses. Closed-form analytical solutions for three-dimensional ductile fracture are still not available. Nakamura and Parks (1990) investigated the stress fields near the front of a through-thickness crack in a thin ductile plate employing ABAQUS software. These authors argued that the loss of HRR-dominance at higher load occurs when the finite deformation region outgrows the plane strain region. Guo (1993) presented a structure of stress fields near the front of a crack in a ductile material under tension and introduced T_z as a parameter to characterize the out-of-plane constraint effect. Faleskog (1995) investigated the effect of local constraint along crack fronts on cleavage fracture and ductile fracture using numerical and experimental methods. The author concluded that ductile crack growth initiation

appears to be insensitive to the local constraint, but cleavage crack growth initiation is sensitive to the constraint. Yuan and Brocks (1998) investigated the effects of in-plane and out-of-plane constraints on the stress fields near the front of a crack in a ductile plate using a modified boundary layer model. Their numerical results showed that the local hydrostatic stress ahead of the crack front is a linear function of Q stresses. Kim et al. (2001) performed three dimensional modified boundary layer analyses to study crack-front constraints for a thin ductile plate. These authors argued that in-plane stress fields can be characterized by a J-A_2 three-term solution under small yielding conditions. Roychowdhury and Dodds (2004) investigated the effect of in-plane constraint (T-stress) on three-dimensional fatigue crack closure in the small-scale yielding regime using finite element methods. These authors believed that both negative and positive T-stresses reduce the variation of local opening load levels along the front of a crack in a ductile plate. Carlyle and Dodds (2007) studied three-dimensional effects on the fatigue crack closure in a cracked plate under fully-reversed loading using finite element methods. These authors revealed that the magnitude of K_{op}/K_{max} along the crack front remains unchanged when $K_{max}/\sigma_0 B^{0.5}$ is a fixed value. Here, B is the plate thickness, σ_0 is the material yield stress, K_{op} is the crack opening load and K_{max} is the peak load. Alizadeh et al. (2007) made a comparison of two and three-dimensional analyses of fatigue crack closure. These authors revealed that the finite element plane stress and strip yield results agree with the three-dimensional finite element crack opening results for the surface, for all thicknesses. Wang (2009) performed three-dimensional finite element analyses to

examine elastic–plastic crack front fields in a plate with a semi-elliptical surface crack under remote uniaxial and biaxial tension loading. The author concluded that the *J–Q* characterization provides good estimate of the constraint loss for crack front stress fields. Camas et al. (2010) performed numerical study on the thickness transition in bi-dimensional specimen cracks. These authors revealed that the evolution of the plastic zone size at the crack plane along the thickness is strongly dependent of the specimen thickness. Sobotka and Dodds (2011) performed finite element analyses to investigate key features of the elastic–plastic fields near the front of a steadily advancing crack in a thin plate under small-scale yielding conditions. Their numerical results revealed three-dimensional effects extend to a distance of about 1.5–2.5 times the plate thickness ahead of the advancing crack front on the mid-plane. Considering single-edge cracked specimens subjected to general loading, Wang et al. (2014) investigated the effects of the size of these specimens and crack-front constraints on crack front stress fields using finite element methods. Shlyannikov et al. (2014) investigated fracture toughness and in-plane and out-of-plane constraint effects using experimental and numerical methods for high-strength carbon steel 34XH3MA. These authors believed that elastic–plastic stress intensity factors can be used to characterize the material fracture resistance properties. Nikishkov and Matvienko (2016) investigated the effects of plate thickness and strain hardening exponents on the constraint parameter *A* for edge cracked ductile plates under tension using finite element methods. These authors concluded the minimum value of *A* appears on the specimen mid-plane and the value of *A* considerably increases when approaching the

specimen free surface. Recently, Hou (2018) presented a three-dimensional re-meshing technique and investigated the crack closure phenomenon in cracked ductile plates with various thicknesses. The author revealed that the surface effects on crack opening behavior reach a depth that is about 1.34 times the plastic zone size measured by Irwin's approach.

There are many numerical analyses of three-dimensional ductile fracture in the papers mentioned above. However, there are a very limited number of analytical solutions available for three-dimensional ductile fracture because of the mathematical complexities encountering in solving this kind of 3D problems. In the current paper, a semi-analytical method is presented to obtain solutions for crack front fields in a thin ductile plate under tension.

2 Basic equations

Stress components related to three-dimensional Maxwell functions (ϕ_i, i = 1, 2, 3) in a rectilinear coordinate system (shown in Fig.1) may be expressed as

$$\left.\begin{aligned} &\sigma_x = \frac{\partial^2 \phi_2}{\partial z^2} + \frac{\partial^2 \phi_3}{\partial y^2}, \sigma_y = \frac{\partial^2 \phi_1}{\partial z^2} + \frac{\partial^2 \phi_3}{\partial x^2}, \sigma_z = \frac{\partial^2 \phi_1}{\partial y^2} + \frac{\partial^2 \phi_2}{\partial x^2}, \\ &\sigma_{xy} = -\frac{\partial^2 \phi_3}{\partial x \partial y}, \sigma_{xz} = -\frac{\partial^2 \phi_2}{\partial x \partial z}, \sigma_{yz} = -\frac{\partial^2 \phi_1}{\partial y \partial z}. \end{aligned}\right\} \quad (1)$$

The stress components in a cylindrical coordinate system (shown in Fig.1) may be expressed as

$$
\left.\begin{aligned}
\sigma_r &= \cos^2\theta\frac{\partial^2\phi_2}{\partial z^2}+\sin^2\theta\frac{\partial^2\phi_1}{\partial z^2}+\frac{1}{r}(\phi_3)'+\frac{1}{r^2}(\phi_3)'',\\
\sigma_\theta &= \sin^2\theta\frac{\partial^2\phi_2}{\partial z^2}+\cos^2\theta\frac{\partial^2\phi_1}{\partial z^2}+(\phi_3)'',\\
\sigma_{r\theta} &= -\frac{\sin 2\theta}{2}\left(\frac{\partial^2\phi_2}{\partial z^2}-\frac{\partial^2\phi_1}{\partial z^2}\right)+\frac{1}{r^2}(\phi_3)'-\frac{1}{r}(\phi_3)',\\
\sigma_z &= \sin^2\theta(\phi_1)''+\frac{2\sin\theta\cos\theta}{r}(\phi_1)'+\frac{\cos^2\theta}{r}(\phi_1)'-\frac{2\sin\theta\cos\theta}{r^2}(\phi_1)'+\frac{\cos^2\theta}{r^2}(\phi_1)''+\\
&\quad \cos^2\theta(\phi_2)''-\frac{2\sin\theta\cos\theta}{r}(\phi_2)'+\frac{\sin^2\theta}{r}(\phi_2)'+\frac{2\sin\theta\cos\theta}{r^2}(\phi_2)'+\frac{\sin^2\theta}{r^2}(\phi_2)'',\\
\sigma_{rz} &= -\sin\theta\left(\sin\theta\frac{\partial(\phi_1)'}{\partial z}+\frac{\cos\theta}{r}\frac{\partial(\phi_1)'}{\partial z}\right)-\cos\theta\left(\cos\theta\frac{\partial(\phi_2)'}{\partial z}-\frac{\sin\theta}{r}\frac{\partial(\phi_2)'}{\partial z}\right),\\
\sigma_{\theta z} &= -\cos\theta\left(\sin\theta\frac{\partial(\phi_1)'}{\partial z}+\frac{\cos\theta}{r}\frac{\partial(\phi_1)'}{\partial z}\right)+\sin\theta\left(\cos\theta\frac{\partial(\phi_2)}{\partial z}-\frac{\sin\theta}{r}\frac{\partial(\phi_2)'}{\partial z}\right).
\end{aligned}\right\} \tag{2}
$$

Here, $(\ )' = \frac{\partial}{\partial\theta}$ and $(\ )' = \frac{\partial}{\partial r}$.

It can be proved that Eq. (2) meets equilibrium conditions in a cylindrical coordinate system, which can be written as

$$
\left.\begin{aligned}
(\sigma_r)'+\frac{1}{r}(\sigma_{r\theta})'+\frac{\partial\sigma_{rz}}{\partial z}+\frac{\sigma_r-\sigma_\theta}{r}=0,\\
(\sigma_{r\theta})'+\frac{1}{r}(\sigma_\theta)'+\frac{\partial\sigma_{\theta z}}{\partial z}+\frac{2\sigma_{r\theta}}{r}=0,\\
(\sigma_{rz})'+\frac{1}{r}(\sigma_{\theta z})'+\frac{\partial\sigma_z}{\partial z}+\frac{\sigma_{rz}}{r}=0.
\end{aligned}\right\} \tag{3}
$$

Disregarding elastic deformations, the stress-strain relation of hardening materials may be written as

$$
\varepsilon_{ij} = \frac{3}{2E\sigma_0^{n-1}}\alpha\sigma_e^{n-1}s_{ij}. \tag{4}
$$

Here,

$$
s_{ij} = \sigma_{ij}-\frac{1}{3}\sigma_{kk}\delta_{ij}, \tag{5}
$$

$$\sigma_e^2 = \frac{3}{2} s_{ij} s_{ij}, \tag{6}$$

σ_0 represents the yielding stress, E is Young's modulus, α is a material constant and n represents the strain hardening coefficient.

3. Semi-analytical solutions for crack-front fields

3.1 Expressions of stress and strain components

Consider a thin plate containing a through-thickness crack under remote tension, as shown in Fig. 1. The stress functions are attempted in the form

$$\left.\begin{aligned} &\phi_3 = \phi = K(r,z) r^s \tilde{\phi}(r,z,\theta), \\ &\phi_1 = \phi_2 = T_z(r,z)\phi = T_z(r,z) K r^s \tilde{\phi}, \\ &r \to 0. \end{aligned}\right\} \tag{7}$$

Here, K is the plastic stress intensity function, s is the exponent related to plastic singularities, $\tilde{\phi}$ is the function related to angular distributions of stress.

Substituting Eq. (7) into Eq. (2) and disregarding the terms containing r^s and r^{s-1}, one may obtain stress components, written as

$$\left.\begin{aligned} &\sigma_r = \frac{1}{r}(\phi)' + \frac{1}{r^2}(\phi)'' = K r^{s-2}\left(s\tilde{\phi} + \tilde{\phi}''\right) = K r^{s-2}\tilde{\sigma}_r, \\ &\sigma_\theta = (\phi)'' = K r^{s-2} s(s-1)\tilde{\phi} = K r^{s-2}\tilde{\sigma}_\theta, \\ &\sigma_z = (\phi_1)'' + \frac{1}{r}(\phi_1)' + \frac{1}{r^2}(\phi_1)'' = T_z K r^{s-2}\left(\tilde{\phi}'' + s^2\tilde{\phi}\right) = T_z K r^{s-2}\tilde{\sigma}_z, \\ &\sigma_{r\theta} = \frac{1}{r^2}(\phi)' - \frac{1}{r}(\phi)'' = K r^{s-2}(1-s)\tilde{\phi}' = K r^{s-2}\tilde{\sigma}_{r\theta}, \\ &\sigma_{rz} = \sigma_{\theta z} = 0. \end{aligned}\right\} \tag{8}$$

Here, T_z is the out-of-plane constraint level and may be defined by

$$T_z = \frac{\sigma_z}{\sigma_r + \sigma_\theta}. \tag{9}$$

Substituting Eq. (8) into Eq. (4), the strain components near the crack front may be

written as

$$\left.\begin{aligned}
\varepsilon_r &= \frac{\alpha}{2E\sigma_0^{n-1}}\sigma_e^{n-1}\left(\left(2-T_z\right)\left(\frac{1}{r}\phi'+\frac{1}{r^2}\phi''\right)-\left(1+T_z\right)\phi''\right)\\
&= \frac{\alpha}{2E\sigma_0^{n-1}}K^n r^{(s-2)n}\tilde{\sigma}_e^{n-1}\left(\left(2-T_z\right)\left(s\tilde{\phi}+\left(\tilde{\phi}\right)''\right)-\left(1+T_z\right)s\left(s-1\right)\tilde{\phi}\right),\\
\varepsilon_\theta &= \frac{\alpha}{2E\sigma_0^{n-1}}\sigma_e^{n-1}\left(\left(2-T_z\right)\phi''-\left(1+T_z\right)\left(\frac{1}{r}\phi'+\frac{1}{r^2}\phi''\right)\right)\\
&= \frac{\alpha}{2E\sigma_0^{n-1}}K^n r^{(s-2)n}\tilde{\sigma}_e^{n-1}\left(\left(2-T_z\right)s\left(s-1\right)\tilde{\phi}-\left(1+T_z\right)\left(s\tilde{\phi}+\left(\tilde{\phi}\right)''\right)\right),\\
\varepsilon_z &= \frac{\alpha}{2E\sigma_0^{n-1}}\sigma_e^{n-1}\left(2T_z-1\right)\left(\frac{1}{r}\phi'+\frac{1}{r^2}\phi''+\phi''\right)\\
&= \frac{\alpha}{2E\sigma_0^{n-1}}\left(2T_z-1\right)K^n r^{(s-2)n}\tilde{\sigma}_e^{n-1}\left(s^2\tilde{\phi}+\left(\tilde{\phi}\right)''\right),\\
\varepsilon_{r\theta} &= -\frac{3\alpha}{2E\sigma_0^{n-1}}\sigma_e^{n-1}\left(\frac{1}{r}\phi''-\frac{1}{r^2}\phi'\right)=\frac{3\alpha}{2E\sigma_0^{n-1}}K^n r^{(s-2)n}\tilde{\sigma}_e^{n-1}\left(1-s\right)\left(\tilde{\phi}\right)',\\
\varepsilon_{rz} &= 0, \varepsilon_{\theta z}=0.
\end{aligned}\right\} \tag{10}$$

Here,

$$\begin{aligned}
\sigma_e &= \sqrt{\frac{3}{2}\left[\left(\sigma_\theta-\frac{1+T_z}{3}\left(\sigma_\theta+\sigma_r\right)\right)^2+\left(\sigma_r-\frac{1+T_z}{3}\left(\sigma_\theta+\sigma_r\right)\right)^2\right.}\\
&\quad\left.+\left(\sigma_z-\frac{1+T_z}{3}\left(\sigma_\theta+\sigma_r\right)\right)^2+2\left(\sigma_{r\theta}\right)^2\right]\\
&= Kr^{s-2}\tilde{\sigma}_e
\end{aligned} \tag{11}$$

and

$$\begin{aligned}
\tilde{\sigma}_e &= \sqrt{\frac{3}{2}\left[\left(s\left(s-1\right)\tilde{\phi}-\frac{1+T_z}{3}\left(s^2\tilde{\phi}+\left(\tilde{\phi}\right)''\right)\right)^2+\left(\frac{2T_z-1}{3}\left(s^2\tilde{\phi}+\left(\tilde{\phi}\right)''\right)\right)^2\right.}\\
&\quad\left.+\left(s\tilde{\phi}+\left(\tilde{\phi}\right)''-\frac{1+T_z}{3}\left(s^2\tilde{\phi}+\left(\tilde{\phi}\right)''\right)\right)^2+2\left(1-s\right)^2\left(\left(\tilde{\phi}\right)'\right)^2\right].
\end{aligned} \tag{12}$$

3.2 Solution for *s* and the relationship between *J*-integral and *K* in three-dimensional fracture

A *J*-integral in three-dimensional fracture (Kishimoto and Sakata, 1980; Shih et

al., 1986; Chiarelli and Frediani, 1993; Rigby and Aliabadi, 1998; Eriksson, 2000; Omer and Yosibash, 2005) may be written as

$$J(\eta)=\int_{\Gamma_1}\left(Wdy-\sigma_{ij}n_j u_{i,x}ds\right),(r_1\to 0)$$
$$=\int_{\Gamma_2}\left(Wdy-\sigma_{ij}n_j u_{i,x}ds\right)-\int_{A(\Gamma_2)}\frac{\partial\left(\sigma_{iz}u_{i,x}\right)}{\partial z}dA(\Gamma_2),i=x,y,z,\ j=x,y. \tag{13}$$

Here, $J(\eta)$ represents the *J*-integral at a given point η along the crack front as shown in Fig. 2. W is the strain energy density, σ_{ij} and u_i are stress and displacement components separately. Both path Γ_1 and path Γ_2 lie in the plane perpendicular to the crack front, and n_j are the components of a unit vector outward normal to the integral paths and normal to the crack front. A_{Γ_2} represents the region bounded by Γ_2.

The strain energy density *W* near the crack front may be expressed as

$$W=\int_0^{\varepsilon_{ij}}\sigma_{ij}d\varepsilon_{ij}=\frac{\alpha n}{E\sigma_0^{n-1}}\int_0^{\sigma_e}\sigma_e^n d\sigma_e=\frac{\alpha n}{E\sigma_0^{n-1}(n+1)}K^{n+1}r^{(s-2)(n+1)}\tilde{\sigma}_e^{n+1}. \tag{14}$$

Near the crack front, one finds (Hutchinson, 1968)

$$\begin{aligned}\sigma_{ij}n_j u_{i,x}&=\sigma_r\left(\frac{\sin\theta}{r}\left((u_r)^{\square}-u_\theta\right)+(u_r)'\cos\theta\right)+\sigma_{r\theta}\left(-\frac{\sin\theta}{r}\left((u_\theta)^{\square}+u_r\right)+\cos\theta(u_\theta)'\right)\\&=\frac{\alpha}{E\sigma_0^{n-1}}K^{n+1}r^{(s-2)(n+1)}\left\{\sin\theta\left(\tilde{\sigma}_r\left(\tilde{u}_\theta-(\tilde{u}_r)^{\square}\right)-\tilde{\sigma}_{r\theta}\left((\tilde{u}_\theta)^{\square}+\tilde{u}_r\right)\right)\right.\\&\quad\left.+\left(n(s-2)+1\right)\cos\theta\left(\tilde{\sigma}_r\tilde{u}_r+\tilde{\sigma}_{r\theta}\tilde{u}_\theta\right)\right\},\\&i=x,y,z,\ j=x,y.\end{aligned} \tag{15}$$

Here, $\tilde{u}_r$, $\tilde{u}_\theta$, $(\tilde{u}_r)^{\square}$ and $(\tilde{u}_\theta)^{\square}$ can be found in appendix A.

The *J*-integral in three-dimensional fracture may be written as

$$J(z)=\int_{\Gamma}\left(Wdy-\sigma_{ij}n_j u_{i,x}ds\right)=\frac{\alpha}{E\sigma_0^{n-1}}K^{n+1}r^{(s-2)(n+1)+1}I,(r\to 0),$$
$$I(T_z,n)=\int_{-\pi}^{\pi}\left\{\frac{n}{n+1}(\tilde{\sigma}_e)^{n+1}\cos\theta\right.$$
$$\left.-\left(\sin\theta\left(\tilde{\sigma}_r\left(\tilde{u}_\theta-(\tilde{u}_r)'\right)-\tilde{\sigma}_{r\theta}\left((\tilde{u}_\theta)'+\tilde{u}_r\right)\right)+\cos\theta\left((s-2)n+1\right)\left(\tilde{\sigma}_r\tilde{u}_r+\tilde{\sigma}_{r\theta}\tilde{u}_\theta\right)\right)\right\}d\theta. \tag{16}$$

The value of the *J*-integral should not be zero or infinity when *r* tends to zero. Hence, one may have

$$\left.\begin{aligned}&J(z)=\frac{\alpha}{E\sigma_0^{n-1}}K^{n+1}I,\\&s=\frac{2n+1}{n+1}.\end{aligned}\right\} \tag{17}$$

3.2 Solutions for $\tilde{\phi}$

Based on the principle of minimum complementary potential energy and using variational methods, one may obtain the equation with the strain components near the crack front should meet, expressed as

$$\left((r\varepsilon_\theta)''+\frac{(\varepsilon_r)'}{r}-(\varepsilon_r)'-(\gamma_{r\theta})'-\left(\frac{\gamma_{r\theta}}{r}\right)'\right)+T_z\left(\frac{1}{r}(\varepsilon_z)'+(\varepsilon_z r)''-(\varepsilon_z)'\right)=0 \tag{18}$$

Specially, for plane stress (T_z =0) and plane strain (ε_z = 0), only the terms in the first bracket appear. The derivation of Eq. (18) is shown in appendix B.

Substituting the strain components (Eq. (10)) into Eq. (18), one may obtain

$$A\left(\sigma_e^{n-1}\right)''+B\left(\sigma_e^{n-1}\right)'''+C\left(\sigma_e^{n-1}\right)''+D\left(\sigma_e^{n-1}\right)'+E\left(\sigma_e^{n-1}\right)'+F\sigma_e^{n-1}=0. \tag{19}$$

Here,

$$
\left.\begin{aligned}
A &= 2r\phi'' - \phi' - \frac{\phi'''}{r} + 2\left(T_z - 1\right)T_z\left(r\phi'' + \phi' + \frac{\phi'''}{r}\right),\\
B &= -\frac{\phi''}{r} + \frac{2\phi'}{r^2} + \frac{2\phi'''}{r^3} + 2\left(T_z - 1\right)T_z\left(\frac{\phi''}{r} + \frac{\phi'}{r^2} + \frac{\phi'''}{r^3}\right),\\
C &= 6\left(\frac{\phi''}{r} - \frac{\phi'}{r^2}\right),\\
D &= 4r\phi''' + 3\phi'' + \frac{4\phi'''}{r} - \frac{2\phi'}{r} - \frac{6\phi'''}{r^2} + 2\left(T_z - 1\right)T_z\left(2r\phi''' + 3\phi'' + \frac{2\phi'''}{r} - \frac{\phi'}{r} - \frac{3\phi'''}{r^2}\right),\\
E &= \frac{4\phi''''}{r} - \frac{2\phi'''}{r^2} + \frac{4\phi''''}{r^3} + \frac{6\phi''}{r^3} + 4\left(T_z - 1\right)T_z\left(\frac{\phi''''}{r} + \frac{\phi'''}{r^2} + \frac{\phi''''}{r^3}\right),\\
F &= 2\left(\left(T_z - 1\right)T_z + 1\right)\left(r\phi''''' + 2\phi''''' + \frac{2\phi''''}{r} - \frac{\phi'''}{r} - \frac{2\phi''''}{r^2} + \frac{\phi''}{r^2} + \frac{4\phi'''}{r^3} + \frac{\phi''''}{r^3}\right).
\end{aligned}\right\} \tag{20}
$$

Here, only terms containing $r^{(s-2)n-1}$ are kept. Further, substituting Eq. (11) and Eq.(12) into Eq. (19) and only keeping the terms containing $r^{(s-2)n-1}$, one may obtain the resulting equation, expressed as

$$
\begin{aligned}
\tilde{\phi}'''' = \frac{1}{H}\Big[& \tilde{B}(n-1)\left((n-3)\frac{1}{4\tilde{\sigma}_e^2}\left(\left(\tilde{\sigma}_e^2\right)'\right)^2 + \frac{1}{2}\left(\tilde{\sigma}_e^2\right)^*\right)\\
& + \frac{(n-1)}{2}\left(\tilde{C}(s-2)(n-1) + \tilde{E}\right)\left(\tilde{\sigma}_e^2\right)'\\
& + \left(\tilde{A}(s-2)(n-1)\left((s-2)(n-1)-1\right) + \tilde{D}(s-2)(n-1) + \tilde{F}\right)\tilde{\sigma}_e^2\Big].
\end{aligned} \tag{21}
$$

Here, H, $\tilde{A}$, $\tilde{B}$, $\tilde{C}$, $\tilde{D}$, $\tilde{E}$, $\tilde{F}$, $\left(\tilde{\sigma}_e^2\right)'$ and $\left(\tilde{\sigma}_e^2\right)^*$ can be found in appendix A.

When T_z is given, Eq. (21) may be solved using a fourth-order Runge-Kutta method. Following Hutchison's paper (Hutchinson, 1968), the values of $\tilde{\phi}\big|_{\theta=0}$ and $\tilde{\phi}'''\big|_{\theta=0}$ can be determined when stress-free boundary conditions and an additional condition implying $\max\{\tilde{\sigma}_e\}=1$ are met at the same time. The stress-free boundary conditions require

$$
\tilde{\phi}(\pm\pi) = \tilde{\phi}'(\pm\pi) = 0. \tag{22}
$$

The imposed symmetry($(\sigma_{r\theta})_{\theta=0} = (\sigma_r)'_{\theta=0} = (\sigma_\theta)'_{\theta=0} = (\sigma_z)'_{\theta=0} = 0$) requires

$$\tilde{\phi}'''(0)=\tilde{\phi}''(0)=0\,. \tag{23}$$

4. Three dimensional finite element analyses

To verify the analytical results, finite element analyses are carried out. A cylinder containing a crack front is considered, see Fig. 3(a). The typical boundary layer analysis model has been applied to investigate crack-front stress fields by many researchers (Nakamura and Parks, 1988, 1990; Yuan and Brocks, 1998; Kim et al., 2001; Roychowdhury and Dodds, 2004; Sobotka and Dodds, 2011; Kotousov, 2013). The stress state on the outer circular boundary can be described by the classical William's solution. The radius of the cylinder *a* should be large enough so that the maximum crack front plastic zone is within a linear-elastic (plane-stress) region and has negligible interaction with the outer boundary. The radius *a* also should be much larger than the plate thickness so that the three-dimensional constraint vanishes at the outer boundary. Nakamura and Parks (1990) and Roychowdhury and Dodds (2004) suggested the radius may be taken as 100 times the plate thickness. Yuan and Brocks(1998) and Kim et al. (2001) suggested that the radius is 10 times the plate thickness. In the current paper, the radius *a* is taken as 50 times the plate thickness, i.e., $a=100h$. Only a quarter of the cylinder is modeled considering the symmetry condition and the mesh is constructed with 8-node brick elements, as shown in Fig. 3(b). In the plane perpendicular to the crack front, the element size in the radial direction increases progressively with increasing radial distance *r* from the crack front and the minimum radial size is $10^{-4}h$ at the crack front. There are 36 elements which distribute uniformly in the circumferential direction. The same planar mesh is

repeated along the *z*-axis from the mid-plane (*z*=0) to the free surface (*z*=*h*). The element density increases gradually when approaching the free surface (the ratio is 1.25) considering high stress gradients. There are 25 layers through the half thickness of the plate and the minimum element thickness is $10^{-3}h$ at the free surface, as shown in Fig3(b). The mesh density becomes higher when approaching the crack front. There are 78,300 elements in the region $r<h$ and there are 91,800 elements in the region $r<10h$. The entire mesh consists of 100,800 elements.

Boundary conditions for the current problem may be expressed as

$$\left.\begin{aligned} &u_z\big|_{z=0}=0, u_y\big|_{y=0,x\geq 0}=0,\\ &\sigma_r\big|_{r=a}=\frac{K^{\infty}}{4\sqrt{2\pi a}}\left(5\cos\frac{\theta}{2}-\cos\frac{3}{2}\theta\right),\\ &\sigma_{r\theta}\big|_{r=a}=\frac{K^{\infty}}{4\sqrt{2\pi a}}\left(\sin\frac{\theta}{2}+\sin\frac{3}{2}\theta\right). \end{aligned}\right\} \tag{24}$$

Here, $K^{\infty}=\sqrt{\pi a}\sigma^{\infty}$ and $a=100h$.

In the current FE analyses, Poisson's ratio *v*=0.3, the yield stain $\varepsilon_0=0.002$, α is taken as 1 and the strain hardening coefficients are taken as 3,10 and 13. Here, we use virtual materials. One also may consider real materials. For example, one may suppose that *E* =500GPa and yield stress $\sigma_0 = 0.002E$ =1000MPa.

Undoubtedly, the requirement of the radius *a* limits the application of the finite element model in some practical plates. The current finite element model cannot be applied in following geometric plate dimensions, i.e.,

1. relative short ligaments, e.g., (*W*-*a*)/2h< 0.5,

2. small height to length ratios (*L*/*W*) of the plate,

3. short cracks, e.g., $a/h<1$.

5 Results and discussion

The variation of $J(z)$ normalized by J^{∞} along the crack front at various loading levels is plotted in Fig. 4. The figure shows that the value of J/J^{∞} decreases slowly in the region $0 \leq z/h \leq 0.95$, then drops rapidly when approaching the free surface ($0.95 \leq z/h \leq 1$). The figure also demonstrates that the value of J/J^{∞} increases with increasing loading on the mid-plane.

The variation of T_z near the crack front in the thickness direction at various loading levels is shown in Fig. 5. One may observe the value of T_z increases with increasing loading at all depths. The figure also illustrates the value of T_z decreases slowly with increasing z/h first and then abruptly drops when approaching the free surface at all loading levels. The free-surface dominated region are discussed by some researchers (Nakamura and Parks, 1990; Kotousov, 2010; Camas et al., 2011; Branco et al., 2012). Branco et al. (2012) suggested that the free-surface dominated region may be determined by the criterion that the slope of T_z is larger than 10 in the region (shown in Fig. 6(a)). Based on the criterion, the variation of the thickness of free-surface dominated region normalized by the half thickness (marked t/h) in the radial direction are plotted in Fig. 6(b). Detailed investigations on the stress fields in the free-surface dominated region for a cracked ductile plate are beyond the scope of the current paper due to complexities of the problem.

The variation of T_z in the radial direction on the mid-plane is plotted in Fig. 7.

One may find that T_z tends to zero when $\log_{10}(r/h)$ increases to 0 at all loading levels. This implies the three-dimensional constraint vanishes at a radial distance of about one half of the plate thickness from the crack front on the mid-plane. Fig. 7 also shows the value of T_z tends to 0.5 when r tends to zero. This indicates plane strain conditions may be met approximately at the crack front. Fig. 7 shows that there is a line called elastic line where all curves of T_z terminate when the plastic zone sizes are less than the half-thickness of the plate.

The θ-variation of in-plane stresses normalized by the yield stress near the crack front on the mid-plane and the plane close to the free surface are plotted in Fig. 8 and Fig. 9. These figures show the current analytical results are in agreement with the corresponding FE results. These results verify that the in-plane stresses near the crack front can be characterized by current J-T_z solutions.

Comparisons between HRR-field, FE and analytical results are plotted in Fig. 10. The figure illustrates that the FE results of σ_θ / σ_0 and σ_r / σ_0 near the crack front are larger than the corresponding plane stress HRR-field results but less than the corresponding plane strain HRR-field results. The analytical results are in better agreement with FE results than the corresponding HRR-field results.

The radial variation of normalized opening stress σ_θ / σ_0 ahead of the crack front on the mid-plane at various loading levels is shown in Fig. 11. One may find the normalized opening stresses tend to the corresponding plane strain HRR-field solutions when approaching the crack front. One also finds the normalized opening stresses decrease with increasing $\log_{10}(r/h)$. The analytical results of σ_θ / σ_0 are in

good agreement with the corresponding FE results in the plastic zone at various loading levels, as shown in Fig.11(a), (b), (c) and (d). Both Figs.11(a) and (b) suggest that σ_θ / σ_0 will not tend to the corresponding plane stress solutions in the case of small scale yielding, as already pointed out by other authors. However if the loading is large enough so that the plastic zone size ahead of the crack front on the mid-plane is larger than one half thickness of the plate, one may observe the value of σ_θ / σ_0 decreases gradually from the corresponding plane strain HRR-field solutions to the corresponding plane stress HRR-field solutions with increasing $\log_{10}(r/h)$, as illustrated in Figs. 11(c) and (d).

The results of J, T_z and opening stresses are compared with those given by Nakamura and Parks (1990) and the agreement of these numerical and theoretical results is good, as shown in Fig. 4(b), Fig. 7(b) and Fig. 11(d). The comparison shows the current numerical and theoretical results are valid.

The values of I for various T_z and n are shown in Table. 1. When T_z is taken as 0 or 0.5, the values of I are equal to the corresponding plane stress or strain solutions given by Hutchinson (1968). The value of I increases deceasing hardening coefficient n.

The current semi-analytical approach cannot applied to analyze Mode II and III fracture. Other stress functions, for example, three-dimensional Morera stress functions may be attempted to obtain elastic or plastic solutions for three-dimensional Mode II and III fracture. The work on three-dimensional Mode II and III fracture needs hard theoretical derivations, careful numerical or experimental studies to

confirm or correct the analytical solutions. So, the investigation of Mode II and III fracture does not be carried out in the current paper and may appear in the later work.

6 Summary and conclusions

In the current paper, a semi-analytical method is presented to investigate three-dimensional ductile fracture in a thin hardening plate containing a through-crack under tension. Three-dimensional Maxwell stress functions, the minimum complementary potential energy principle as well as three-dimensional *J*-integrals are used to obtain solutions for the crack front fields. The effect of out-of-plane constraint on the in-plane stress fields near the crack front is examined. Three-dimensional finite element analyses are carried out to validate the current analytical results. This work supports the following conclusions.

1. The in-plane stress fields near the crack front can be characterized by the current J-T_z solutions.

2. The value of normalized *J*-integral J/J^{∞} decreases slowly with increasing normalized depth z/*h* first and then drops rapidly when approaching the free surface. The value J/J^{∞} depends on the applied loading and increases with increasing loading on the mid-plane.

3. The value of out-of-plane constraint level T_z decreases slowly with increasing normalized depth z/*h* first and then drops quickly to zero when approaching the free surface. The value of T_z increases with increasing loading at all depths.

4. The value of T_z tends to 0.5 when approaching the crack front so plane strain

conditions can be met at the crack front except at the corn point. The three-dimensional constraint vanishes at a radial distance of about one half of the plate thickness from the crack front on the mid-plane.

5. Comparison with HRR-field solutions shows that the FE results of σ_θ / σ_0 and σ_r / σ_0 near the crack front are larger than the corresponding plane stress HRR-field results but less than the corresponding plane strain HRR-field results when $0<T_z<0.5$.

6. The value of opening stress tends to the corresponding plane strain HRR-field solutions when approaching the crack front on the mid-plane. If the loading is large enough, one may observe that the normalized opening stress decreases gradually from the corresponding plane strain HRR-field solutions to the corresponding plane stress HRR-field solutions with increasing radial distance *r* from the crack front.

7. The value of *I* increases deceasing hardening coefficient *n*.

References

Alizadeh, H., Hill, D.A., de Matos, P.F.P., Nowell, D., Pavier, M.J., Paynter, R.J., et al., 2007. A comparison of two and three-dimensional analyses of fatigue crack closure. Int. J. Fatigue 29, 222–31. https://doi.org/10.1016/j.ijfatigue.2006.03.014.

Ambati, M., Gerasimov, T., De Lorenzis, L., 2015. Phase-field modeling of ductile fracture. Comput. Mech. 55, 1017-1040. https://doi.org/10.1007/s00466-015-1151-4.

Bazant, Z.P., Estenssoro, L.F., 1979. Surface singularity and crack propagation. Int. J. Solids. Struct. 15, 405–426. https://doi.org/10.1016/0020-7683(79)90062-3.

Benthem, J.P., 1977. State of stress at the vertex of a quarter-infinite crack in a half-space. Int. J. Solids. Struct. 13, 479-492.

https://doi.org/10.1016/0020-7683(77)90042-7.

Betegon, C., Hancock, J.W., 1991. Two parameter characterization of elastic-plastic crack tip fields. J. Appl. Mech. 58, 104–110. https://doi.org/10.1115/1.2897135.

Branco, R., Antunes, F.V., Ricardo, L.C.H., Costa, J.D., 2012. Extent of surface regions near corner points of notched cracked bodies subjected to mode-I loading. Finite Elem. Anal. Des. 50, 147-160. https://doi.org/10.1016/j.finel.2011.09.006.

Burdekin, F.M., Stone, D.E.W., 1966. The crack opening displacement approach to fracture mechanics in yielding materials. J. Strain. Anal. Eng. 1, 145-153. https://doi.org/10.1243/03093247V012145.

Camas, D., Garcia-Manrique, J., Gonzalez-Herrera, A., 2011. Numerical study of the thickness transition in bi-dimensional specimen cracks. Int. J. Fatigue 33, 921-928. https://doi.org/10.1016/j.ijfatigue.2011.02.006.

Carlyle, A.G., Dodds, R.H., 2007. Three-dimensional effects on fatigue crack closure under fully-reversed loading. Eng. Fract. Mech. 74, 457–66. https://doi.org/10.1016/j.engfracmech.2006.06.002.

Chaudhuri, R.A., 2010. Three-dimensional singular stress field at the front of a crack and lattice crack deviation (LCD) in a cubic single crystal plate. Philos. Mag. 90, 2049–2113. https://doi.org/10.1080/14786430903571412.

Chiarelli, M., Frediani, A., 1993. A computation of the three-dimensional J-integral for elastic materials with a view to applications in fracture mechanics. Engng. Fract. Mech. 44, 763-788. https://doi.org/10.1016/0013-7944(93)90205-7.

Conner, R.D., Johnson, W.L., Paton, N.E., Nix, W.D., 2003. Shear bands and cracking

of metallic glass plates in bending. J. Appl. Phys. 94, 904-911. https://doi.org/ 10.1063/1.1582555.

Dugdale, D.S., 1960. Yielding in Steel Sheets Containing Slits. J. Mech. Phys. Solids. 8, 100-104. https://doi.org/10.1016/0022-5096(60)90013-2.

Eriksson, K., 2000. A general expression for an area integral of a point-wise *J* for a curved crack front. Int. J. Fract. 106, 65-80. https://doi.org/10.1023/A:1007646823223.

Faleskog, J., 1995. Effects of local constraint along three-dimensional crack fronts-a numerical and experimental investigation. J. Mech. Phys. Solids. 43, 447-493. https://doi.org/10.1016/0022-5096(94)00067-F.

Goes, D.O., Cesar, R., Castro, P.D., 2014. 3D effects around notch and crack tips. Int. J. Fatigue 62, 159-170. https://10.1016/j.ijfatigue.2013.10.014.

Guo, W., 1993. Elastoplastic three dimensional crack border field-I. Singular structure of the field. Engng. Fract. Mech. 46, 93-104. https://doi.org/10.1016/0013-7944(93)90306-D.

Hartranft, R., Sih, G.C., 1970. An approximate three-dimensional theory of plates with application to crack problems. Int. J. Engng. Sci. 8, 711–729. https://doi.org/10.1016/10.1016/0020-7225(70)90054-6.

He, Z., Kotousov, A., Berto, F., Branco, R., 2016. A brief review of recent three-dimensional studies of brittle fracture. Phys. Mesomech. 19, 6-20. https://doi.org/10.1134/S1029959916010021

Hills, D.A., Kelly, P.A., Dai, D.N., Korsunsky, A.M., 1996. Solution of crack

problems. Kluwer Academic Publisher, Dordrecht.

Hou, C., 2018. Plasticity-induced crack closure from surface to deep interior locations - A three-dimensional finite element study. Engng. Fract. Mech. 195, 186-199. https://doi.org/10.1016/j.engfracmech.2018.04.012.

Hutchinson, J.W., 1968. Singular behaviour at the end of a tensile crack in a hardening material. J. Mech. Phys. Solids. 16, 13-31. https://doi.org/10.1016/0022-5096(68)90014-8.

Hutchinson, J.W., Suo, Z., 1992. Mixed-mode cracking in layered materials. Adv. Appl. Mech. 29, 63–191. https://doi.org/10.1016/S0065-2156(08)70164-9.

Irwin, G.R., 1961. Plastic Zone Near a Crack and Fracture Toughness. Proceedings of Sagamore Research Conference, Syracuse, USA, pp.63-78.

Kim, Y., Zhu, X.K., Chao, Y.J., 2001. Quantification of constraint on elastic-plastic 3D crack front by the J-A_2 three-term solution. Engng. Fract. Mech. 68, 895-914. https://doi.org/10.1016/S0013-7944(00)00134-X.

Kishimoto, K., Aoki, S., Sakata, M., 1980. On the path independent integral-J. Engng. Fract. Mech. 13, 841-881. https://doi.org/10.1016/0013-7944(80)90015-6.

Kotousov, A., 2004. An application of the Kane and Mindlin theory to crack problems in plates of arbitrary thickness. Meccanica 39, 495–509. https://doi.org/10.1007/s11012-004-5735-x.

Kotousov, A., 2007. Fracture in plates of finite thickness. Int. J. Solids. Struct. 44, 8259–8273. https://doi.org/10.1016/j.ijsolstr.2007.06.011.

Kotousov, A., 2010. Effect of plate thickness on stress state at sharp notches and the

strength paradox of thick plates. Int. J. Solids. Struct. 47, 1916–23. https://doi.org/10.1016/j.ijsolstr.2010.03.029.

Kotousov, A., Lazzarin, P., Berto, F., Pook, L.P., 2013. Three-dimensional stress states at crack tip induced by shear and anti-plane loading. Engng. Fract. Mech. 108, 65–74. https://doi.org/10.1016/j.engfracmech.2013.04.010.

Kwon, S.W., Sun, C.T., 2000. Characteristics of three-dimensional stress fields in plates with a through-the-thickness crack. Int. J. Fract. 104, 291–315. https://doi.org/10.1023/a:1007601918058.

Leung, A.Y.T., Su, R.K.L., 1996. Analytical solution for mode I crack orthogonal to free surface. Int. J. Fract. 76, 79–95. https://doi.org/10.1007/BF00034031.

Marsavina, L., Sadowski, T., 2007. Stress intensity factors for an interface kinked crack in a bi-material plate loaded normal to the interface. Int. J. Fract. 145, 237-243. https://doi.org/10.1007/s10704-007-9124-z.

Nakamura, T., Parks, D.M., 1988. Three-dimensional stress field near the crack front of a thin elastic plate. J. Appl. Mech. 55, 805-813. https://doi.org/10.1115/1.3173725.

Nakamura, T., Parks, D.M., 1990. Three-dimensional stress field near the crack front of a thin ductile plate. J. Mech. Phys. Solids. 38, 787-812. https://doi.org/10.1016/0022-5096(90)90040-B.

Nagai, M., Ikeda, T., Miyazaki, N., 2012. Stress intensity factor analysis of a three-dimensional interface crack between dissimilar anisotropic materials under thermal stress. Engng. Fract. Mech. 91, 14–36. https://doi.org/10.1016/j.engfracmech.2012.04.017.

Nikishkov, G.P., Matvienko, Y.G., 2016. Elastic–plastic constraint parameter *A* for test specimens with thickness variation. Fatigue Fract. Eng. Mater. Struct. 39, 939-949. https://doi.org/10.1111/ffe.12390.

O'Dowd, N.P., Shih, C.F., 1992. Family of crack-tip fields characterized by a triaxiality paramcter-II. fracture applications. J. Mech. Phys. Solids. 40, 939-963. https://doi.org/10.1016/0022-5096(92)90057-9.

Omer, N., Yosibash, Z., 2005. On the path independency of the point-wise *J* integral in three-dimensions. Int. J. Fract. 136, 1-36. https://doi.org/10.1007/s10704-005-3934-7.

Pook, L.P., 2013. Five decades of crack path research. Engng. Fract. Mech. 77, 1619-1630. https://doi.org/10.1016/j.engfracmech.2010.04.010.

Rice, J.R., 1968. A path independent integral and the approximate analysis of strain concentration by notches and cracks. J. Appl. Mech. 35, 379-386. https://doi.org/10.1115/1.3601206.

Rice, J.R., 1988. Elastic fracture-mechanics concepts for interfacial cracks. J. Appl. Mech. 55, 98–103. https://doi.org/10.1115/1.3173668.

Rice, J.R., Rosengren, G.F., 1968. Plane strain deformation near a crack tip in a power-law hardening material. J. Mech. Phys. Solids. 16, 1-12. https://doi.org/10.1016/0022-5096(68)90013-6.

Rigby, R.H., Aliabadi, M.H., 1998. Composition of the mixed mode *J*-integral-revisited. Int. J. Solids. Struct. 35, 2073-2099. https://doi.org/10.1016/S0020-7683(97)00171-6.

Ritchie, R.O., Knott, J.F., Rice, J.R., 1973. On the relationship between critical tensile stress and fracture toughness in mild steel. J. Mech. Phys. Solids. 21, 395-410. https://doi.org/10.1016/0022-5096(73)90008-2.

Roychowdhury, S., Dodds, R.H., 2004. Effect of T-stress on fatigue crack closure in 3-D small-scale yielding. Int. J. Solids. Struct. 41, 2581-2606. https://doi.org/10.1016/j.ijsolstr.2003.11.004.

Shih, C.F., Moran, B., Nakamura, T., 1986. Energy release rate along a three-dimensional crack front in a thermally stressed body. Int. J. Fract. 30, 79-102. https://doi.org/10.1007/BF00034019.

Shlyannikov, V.N., Boychenko, N.V., Tumanov, A.V., Fernández-Canteli, A., 2014. The elastic and plastic constraint parameters for three-dimensional problems. Engng. Fract. Mech. 127, 83-96. https://doi.org/10.1016/j.engfracmech.2014.05.015.

Shih, C.F., 1981. Relationship between the j-integral and the crack opening displacement for stationary and extending cracks. J. Mech. Phys. Solids. 29, 305-326. https://doi.org/10.1016/0022-5096(81)90003-x.

Sih, G.C., 1971. A review of the three-dimensional stress problem for a cracked plate. Int. J. Fract. Mech. 7, 39–61. https://doi.org/10.1007/BF00236482.

Sobotka, J.C., Dodds, Jr.R.H., 2011. Steady crack growth in a thin, ductile plate under small-scale yielding conditions: Three-dimensional modeling. Engng. Fract. Mech. 78, 343-363. https://doi.org/10.1016/j.engfracmech.2010.10.006.

Soliman, E., Frederic, D., Moutou, P.R., 2018. A new analytical generalization of the J and G-theta integrals for planar cracks in a three-dimensional medium. Theor. Appl.

Fract. Mech. 94, 101-109. https://doi.org/10.1016/j.tafmec.2018.01.004.

Wang, E., Zhou, W., Shen, G., 2014. Three-dimensional finite element analysis of crack-tip fields of clamped single-edge tension specimens-Part I: Crack-tip stress fields. Engng. Fract. Mech. 116, 122-143. https://doi.org/10.1016/j.engfracmech.2013.10.022.

Wang, X., 2009. Two-parameter characterization of elastic-plastic crack front fields: surface crack plates under tensile loading. Eng. Fract. Mech. 76, 958-982. https://doi.org/10.1016/j.engfracmech.2009.01.002.

Williams, M.L., 1957. On the stress distribution at the base of a stationary crack. J. Appl. Mech. 24, 109–114.

Yang, W., Freund, L.B., 1985. Transverse shear effects for through-cracks in an elastic plate. Int. J. Solids. Struct. 21, 977-994. https://doi.org/10.1016/0020-7683(85)90111-8.

Yi D.K., Wang, T.C., 2018. A new procedure for investigating three-dimensional stress fields in a thin plate with a through-the-thickness crack. Science China-Physics Mechanics & Astronomy 61, 064611. https://doi.org/10.1007/s11433-017-9138-x.

Yuan, H., Brocks, W., 1998. Quantification of constraint effects in elastic-plastic crack front fields. J. Mech. Phys. Solids. 46, 219-241. https://doi.org/10.1016/S0022-5096(97)00068-9.

Xia, L., Wang, T.C., Shih, C.F., 1993. Higher order analysis of crack-tip fields in elastic-plastic power-law hardening materials. J. Mech. Phys. Solids. 41, 665-687. https://doi.org/10.1016/0022-5096(94)90084-1.

Zhou, K., Wei, R., 2014. Modeling cracks and inclusions near surfaces under contact loading. Int. J. Mech. Sci. 83, 163-171. https://doi.org/10.1016/j.ijmecsci.2014.03.028.

Zhou, K., Wei, R., 2015. Semi-Analytic Solution of Multiple Inhomogeneous Inclusions and Cracks in an Infinite Space. Int. J. Comput. Meth. 12, 1550002. https://doi.org/10.1142/s0219876215500024.

Figure Captions

Fig. 1 A thin plate containing a through-thickness crack subjected to remote uniform tensile loading σ^{∞}.

Fig. 2 *J*-integral in three-dimensional fracture.

Fig. 3 (a) Schematic of a thin plate subjected to remote loading and a boundary of a region assumed to be dominated by a plane stress *K*-field, (b) finite element mesh of the quarter-model. Here, $a=100h$.

Fig. 4 Variation of J/J^{∞} along the crack front at various loading levels; (a) for n=3, (b) for n=10, (c) for n=13.

Fig. 5 Variation of out-of-plane constraint T_z in the thickness direction at various loading levels; (a) for n=3, (b) for n=10, (c) for n=13.

Fig. 6 Variation of thickness of the free-surface dominated region normalized by half thickness of the plate (marked t/h) in the radial direction (a) the free-surface dominated region, (b) variation of thickness of the free-surface dominated region in the radial direction.

Fig. 7 Variation of out-of-plane constraint T_z in the radial direction on the mid-plane

at various loading levels; (a) for *n*=3, (b) for *n*=10, (c) for *n*=13.

Fig. 8 θ-variation of in-plane stresses near the crack front normalized by the yielding stress on the mid-plane at various loading levels; ((a) for $J^{\infty}/\sigma_0\varepsilon_0 h = 3.14$ and *n*=3, (b) for $J^{\infty}/\sigma_0\varepsilon_0 h = 0.2$ and *n*=10, (c) for $J^{\infty}/\sigma_0\varepsilon_0 h = 0.084$ and *n*=13, (d) for $J^{\infty}/\sigma_0\varepsilon_0 h = 1.93$ and *n*=13.

Fig. 9 θ-variation of in-plane stresses near the crack front normalized by yielding stress on the plane close to the free surface at various loading levels; (a) for $J^{\infty}/\sigma_0\varepsilon_0 h = 0.084$ and *n*=13, (b) for $J^{\infty}/\sigma_0\varepsilon_0 h = 0.249$ and *n*=13.

Fig. 10 Comparison of HRR-field, FEM and current analytical results near the crack front; (a) for σ_θ/σ_0 on the mid-plane, (b) for σ_r/σ_0 on the mid-plane, (c) for σ_θ/σ_0 on the plane close to the free surface, (d) for σ_r/σ_0 on the plane close to the free surface.

Fig. 11 Variation of opening stress in the radial direction normalized by yielding stress on the mid-plane at various loading levels; (a) for $J^{\infty}/\varepsilon_0\sigma_0 h = 0.248$ and *n*=13, (b) for $J^{\infty}/\varepsilon_0\sigma_0 h = 1.93$ and *n*=13, (c) for $J^{\infty}/\varepsilon_0\sigma_0 h = 10.2$ and *n*=13. (d) for $J^{\infty}/\varepsilon_0\sigma_0 h = 10$ and *n*=10.

Fig. 1

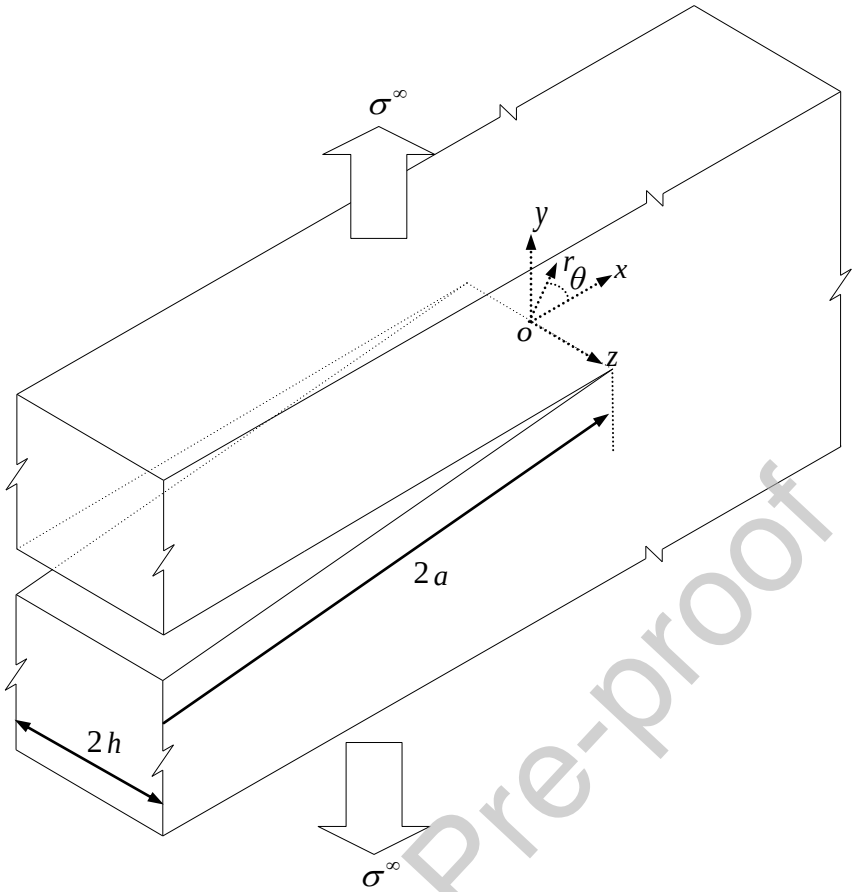

Fig. 2

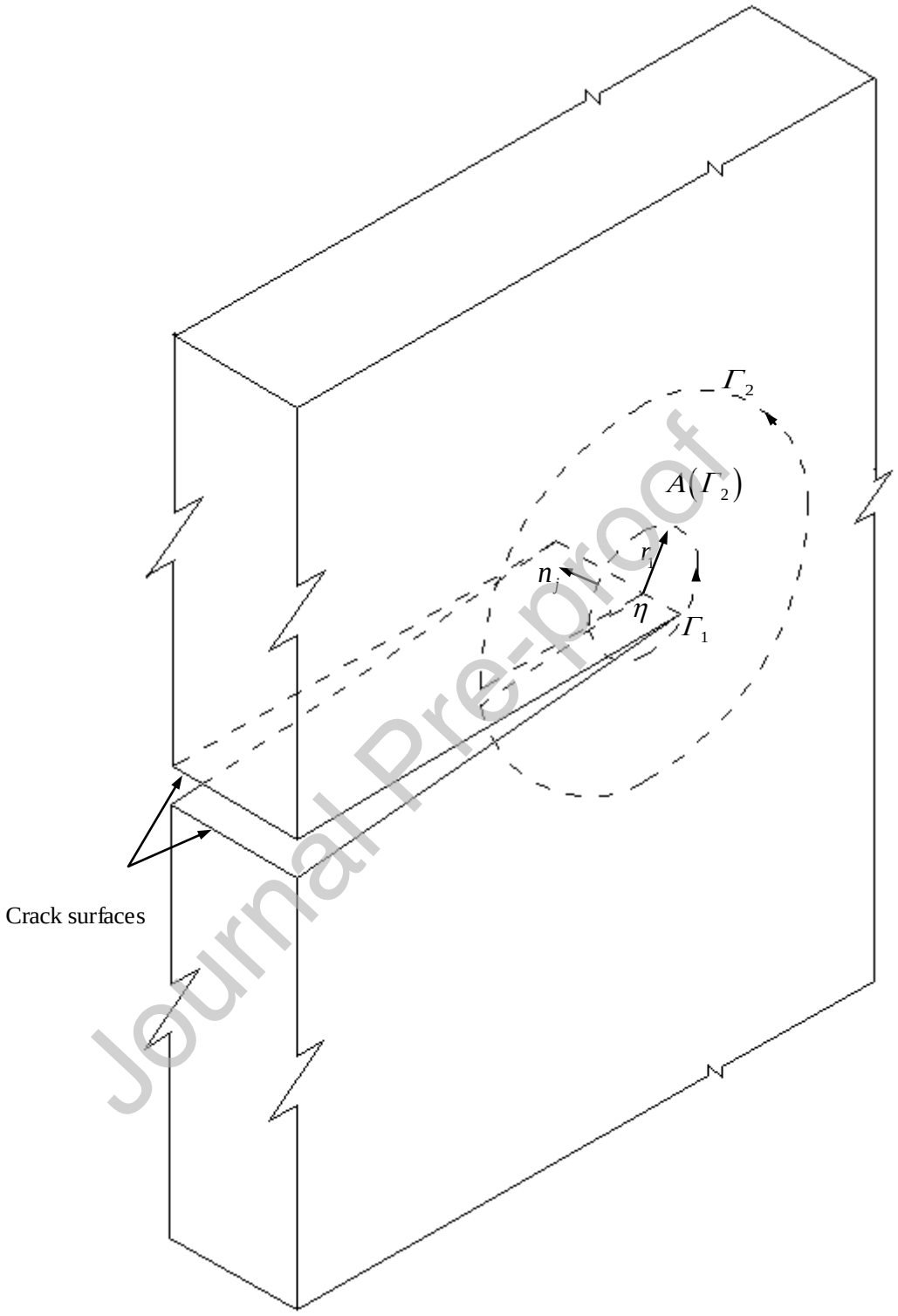

Fig. 3

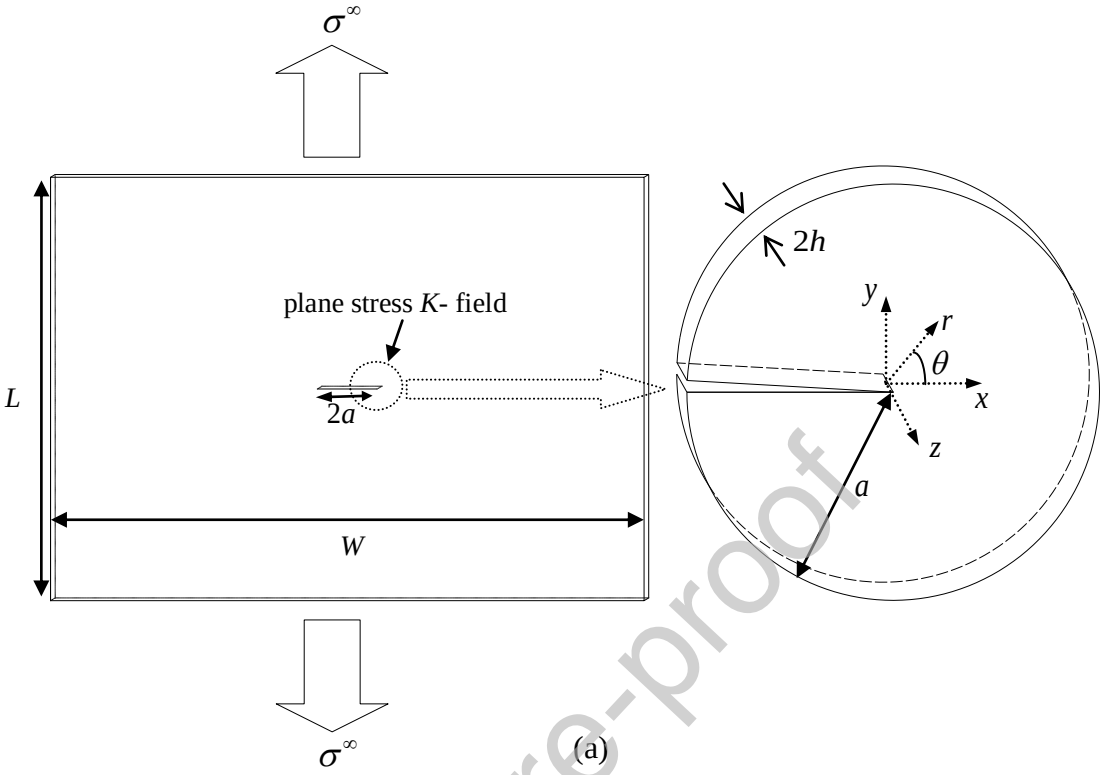

(a)

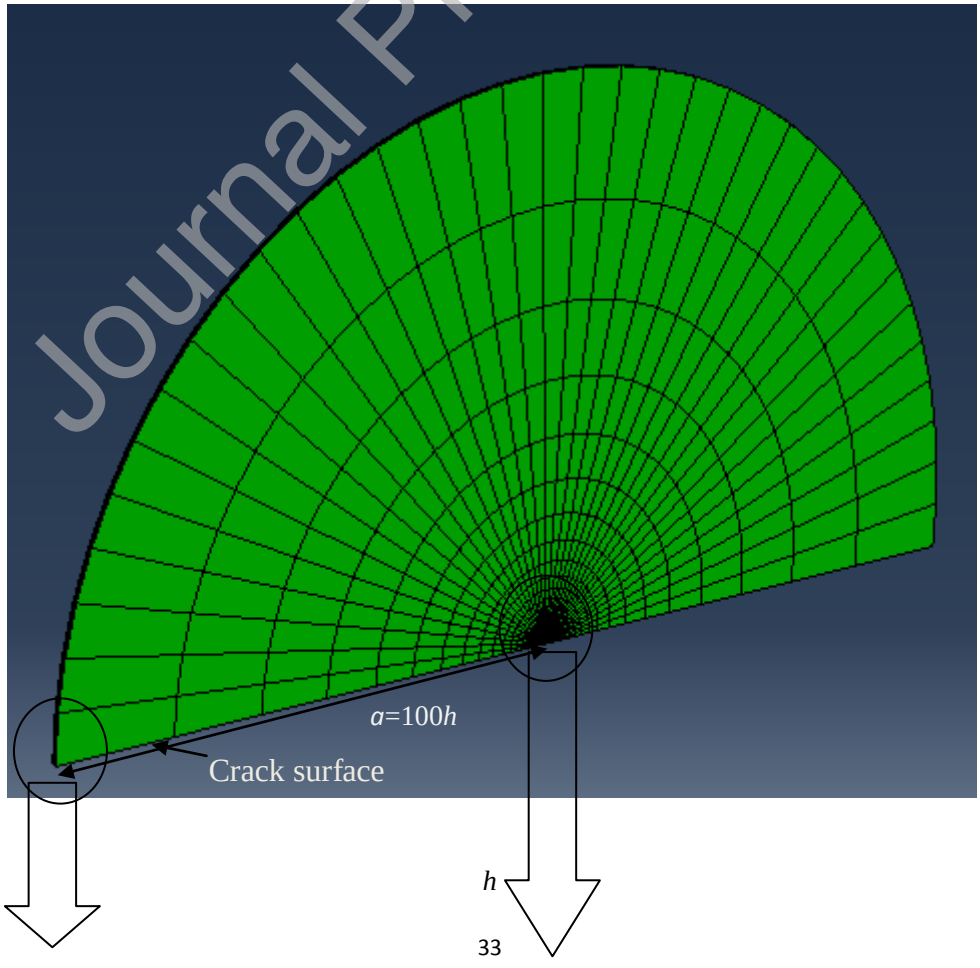

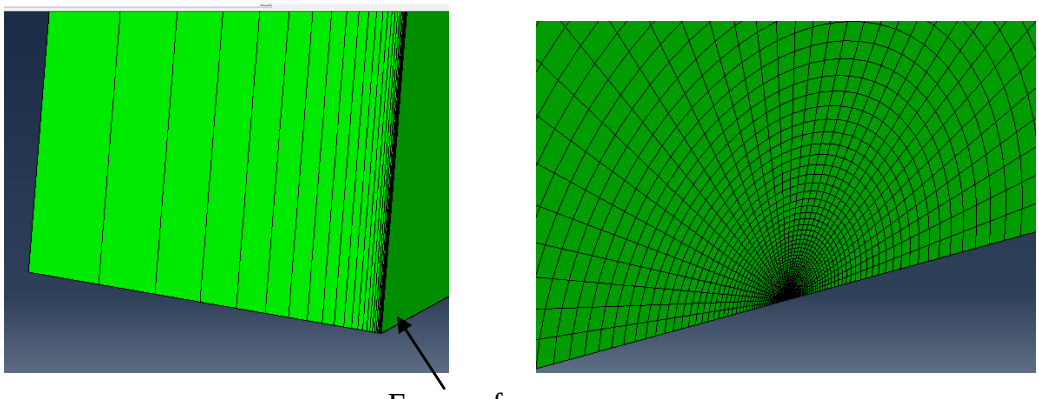

Fig. 4

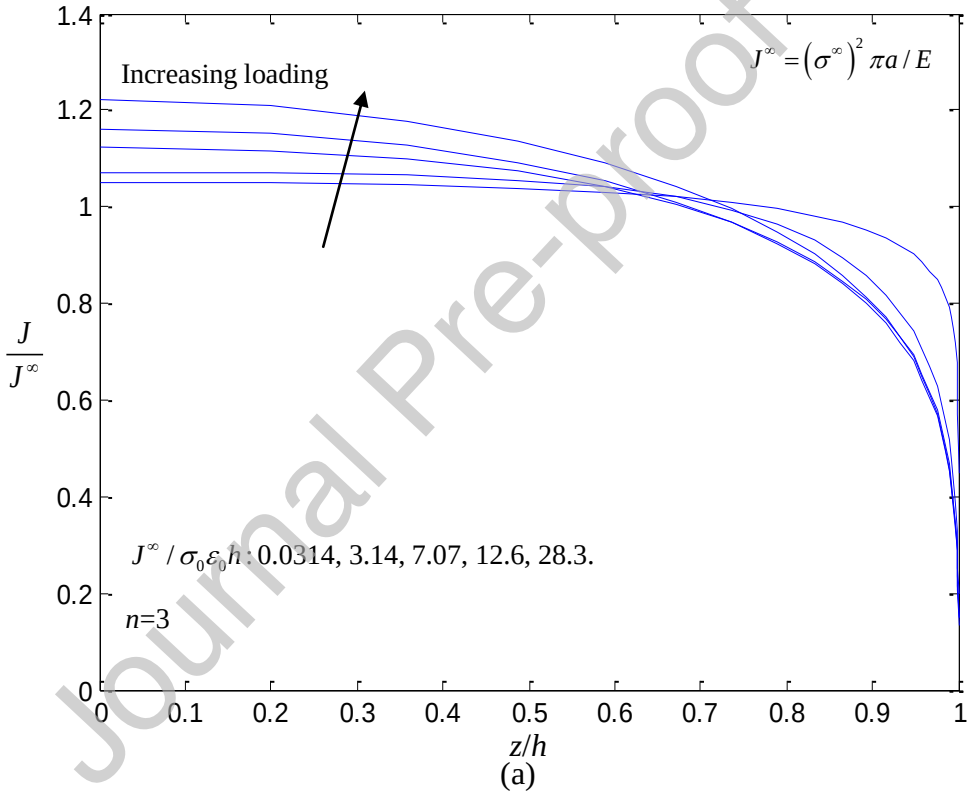

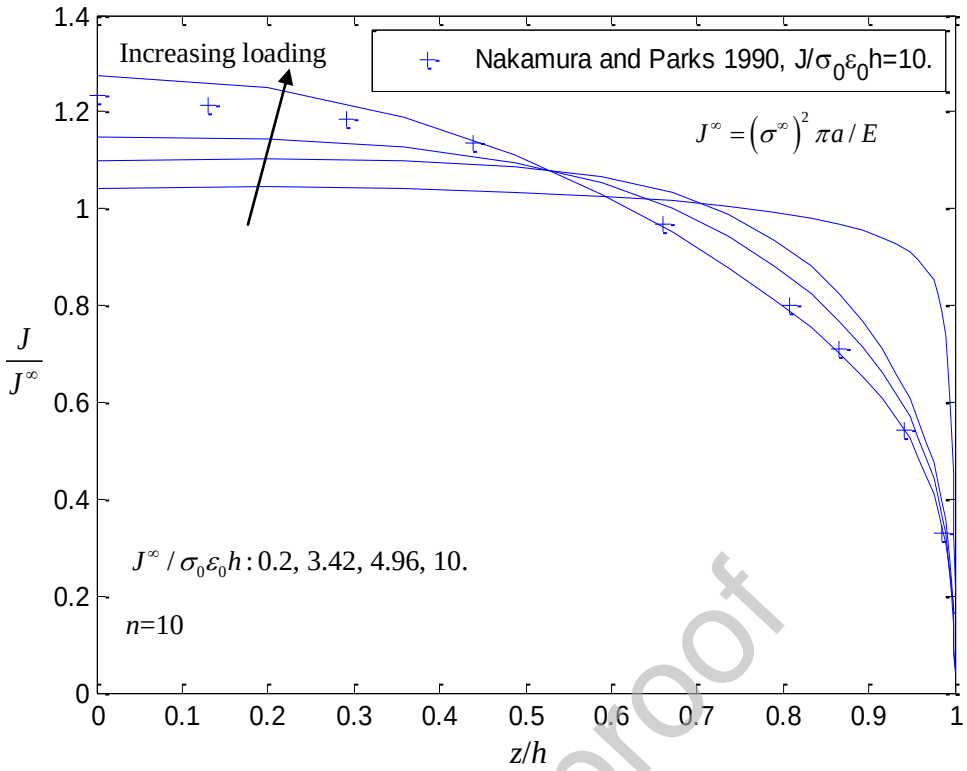

(b)

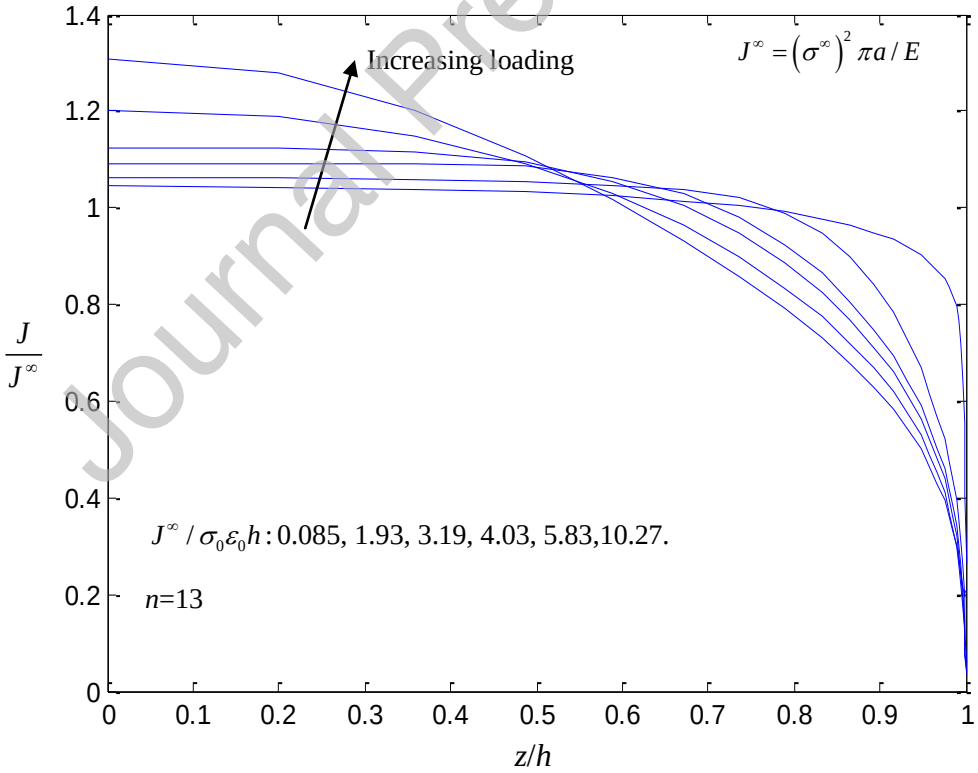

(c)

Fig. 5

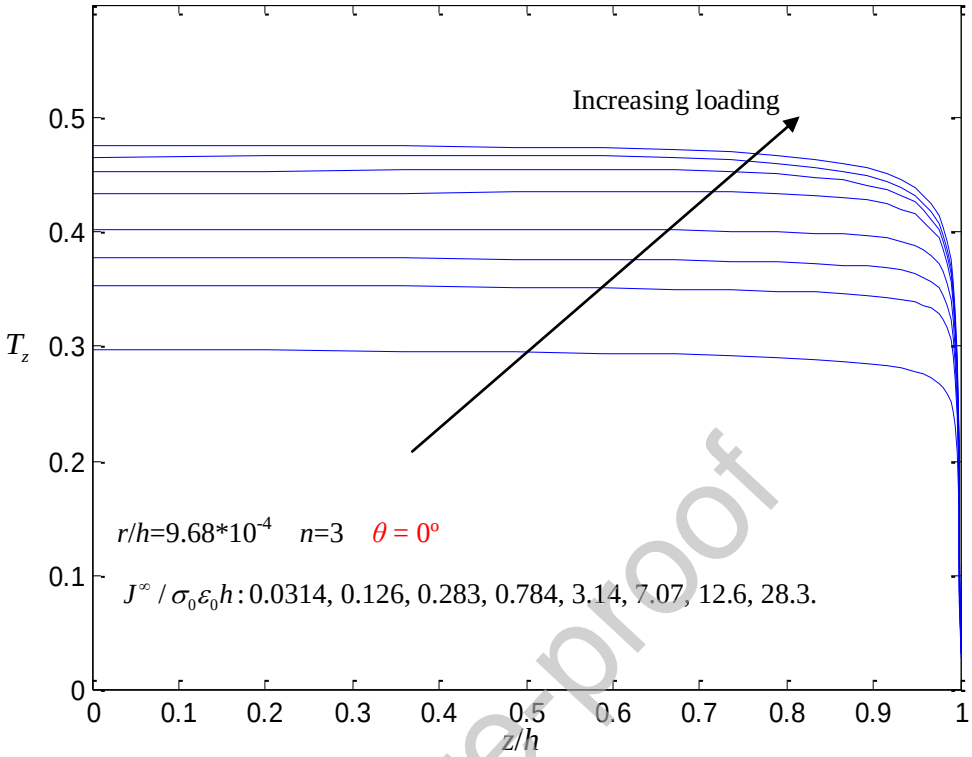

(a)

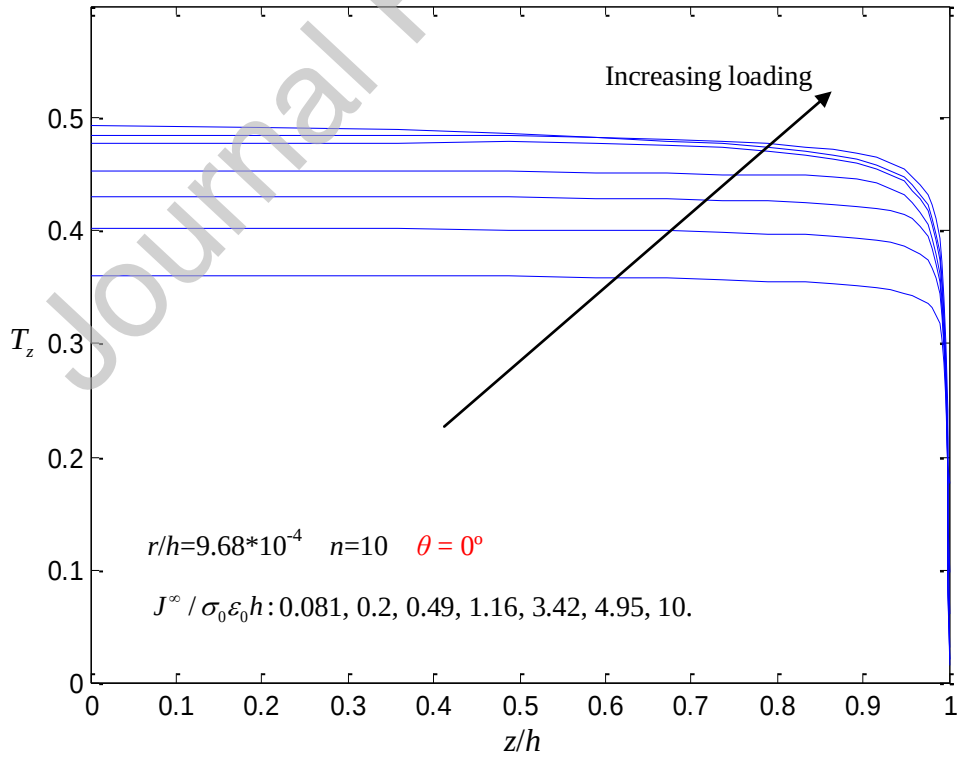

(b)

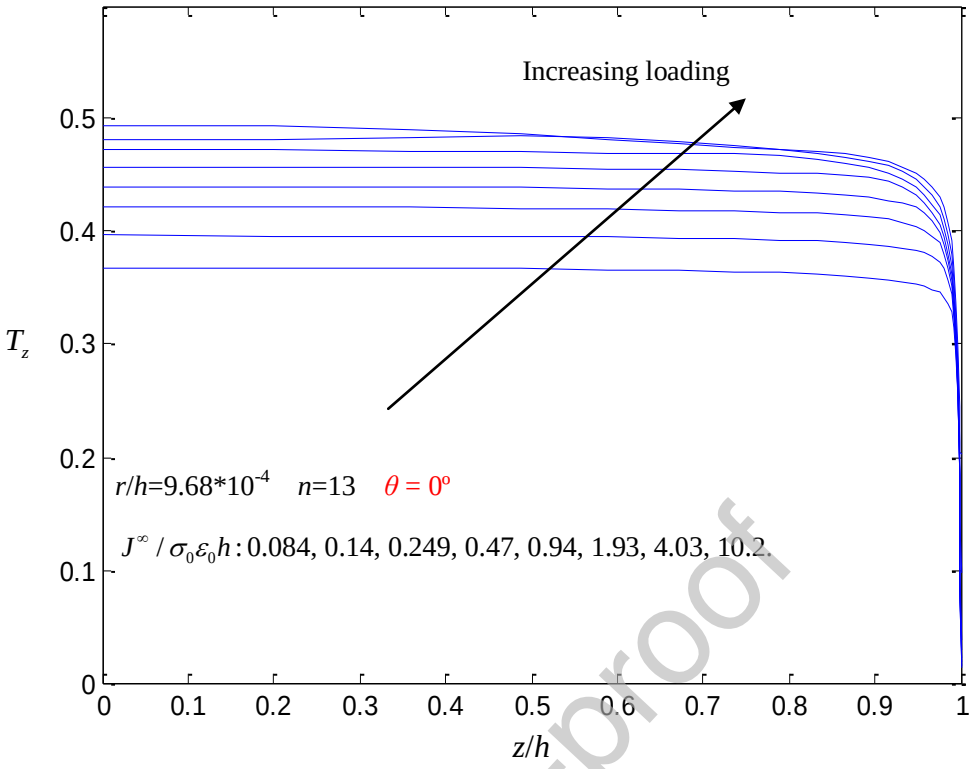

(c)

Fig. 6

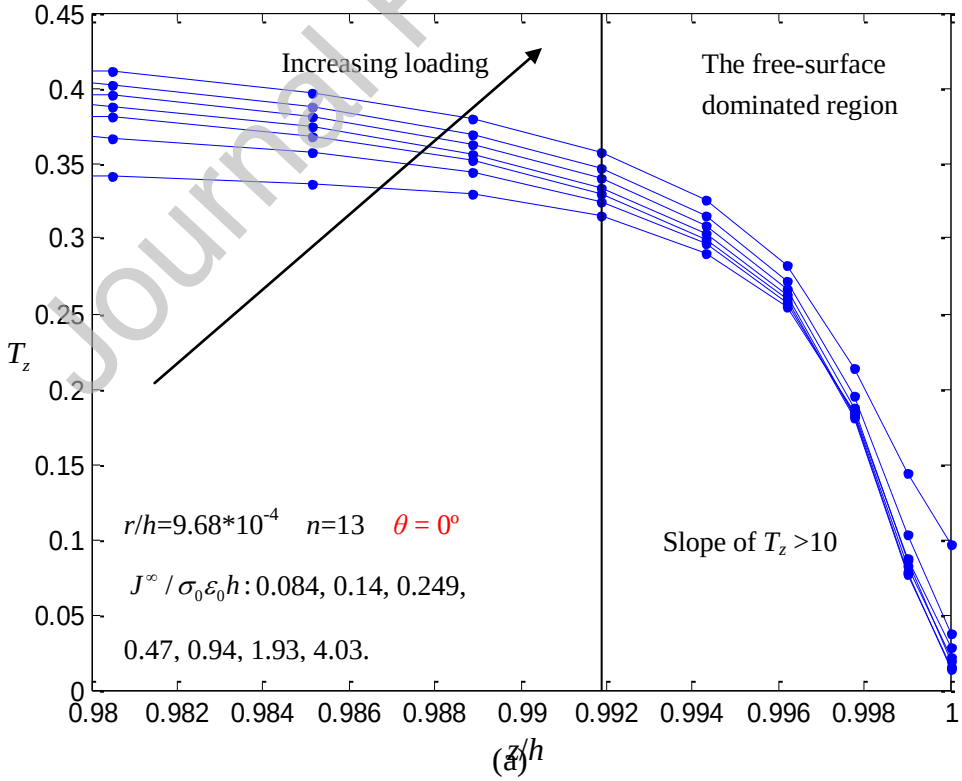

(a)

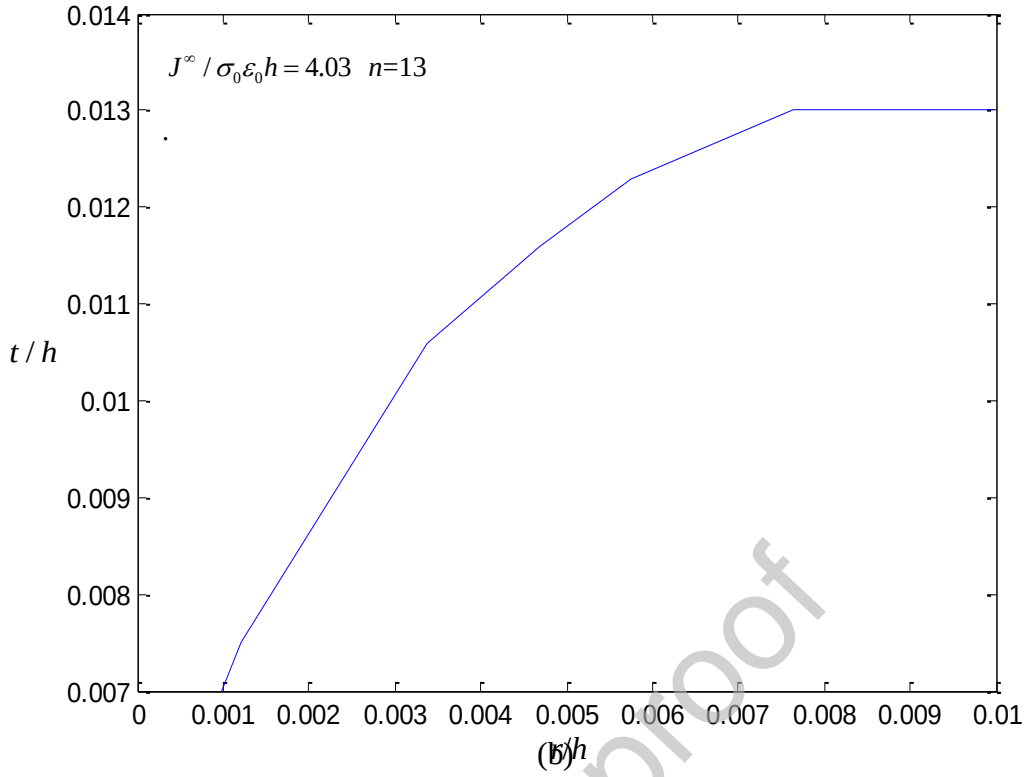

(b)

Fig. 7

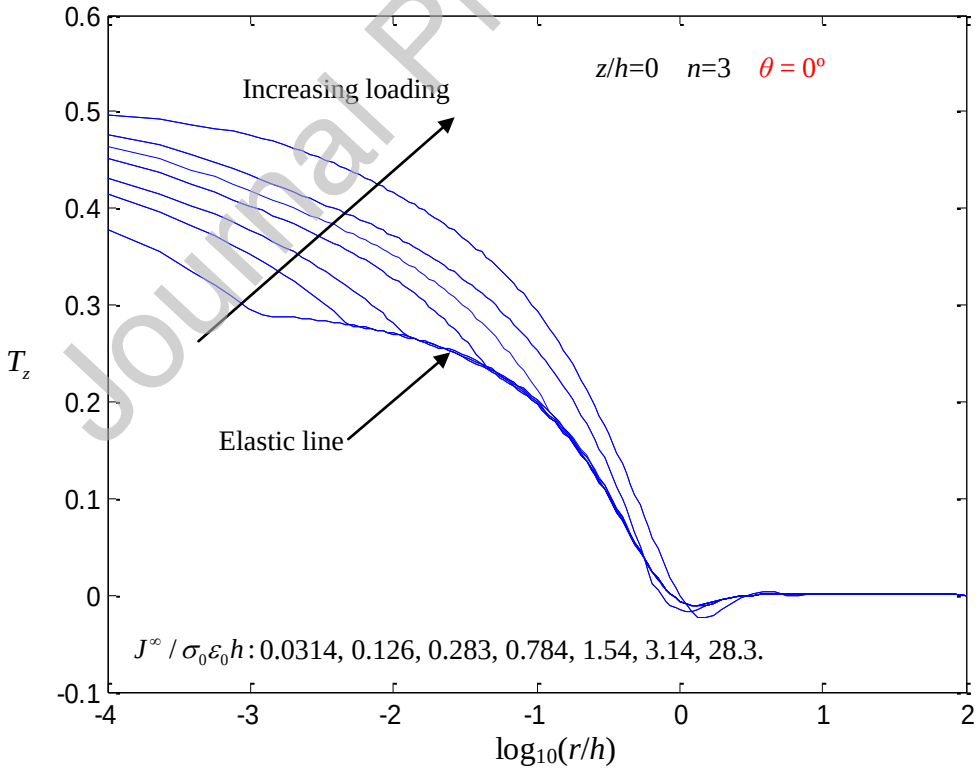

(a)

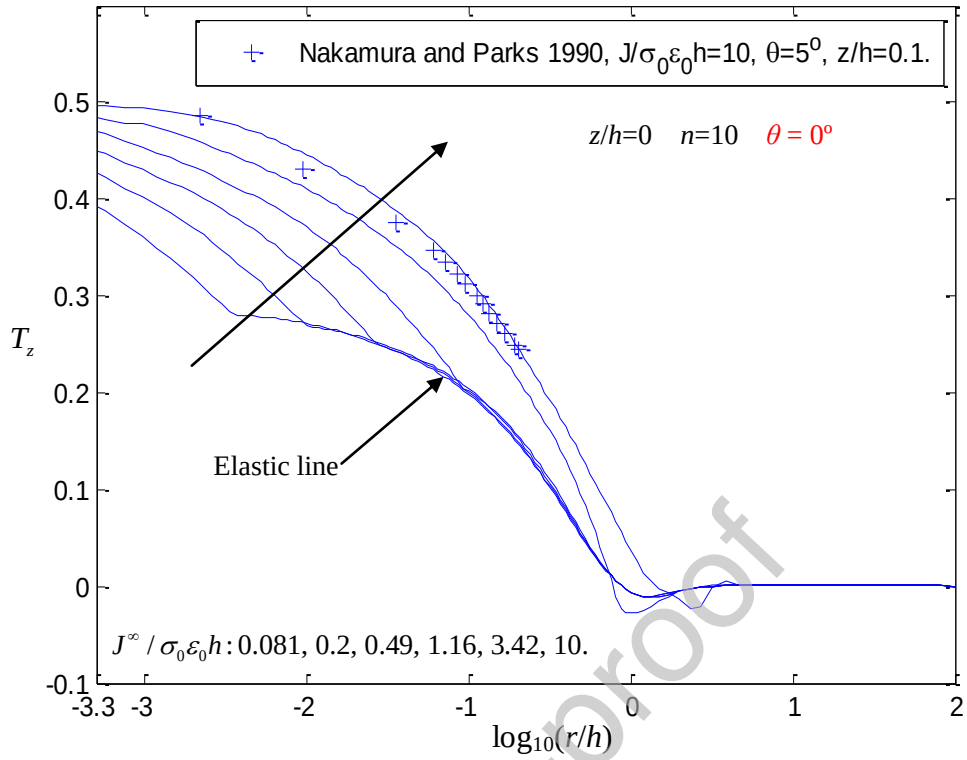
Nakamura and Parks 1990, J/σ0ε0h=10, θ=5o, z/h=0.1.
z/h=0 n=10 θ = 0o
Elastic line
J∞ / σ0ε0h: 0.081, 0.2, 0.49, 1.16, 3.42, 10.
Tz
log10(r/h)

(b)

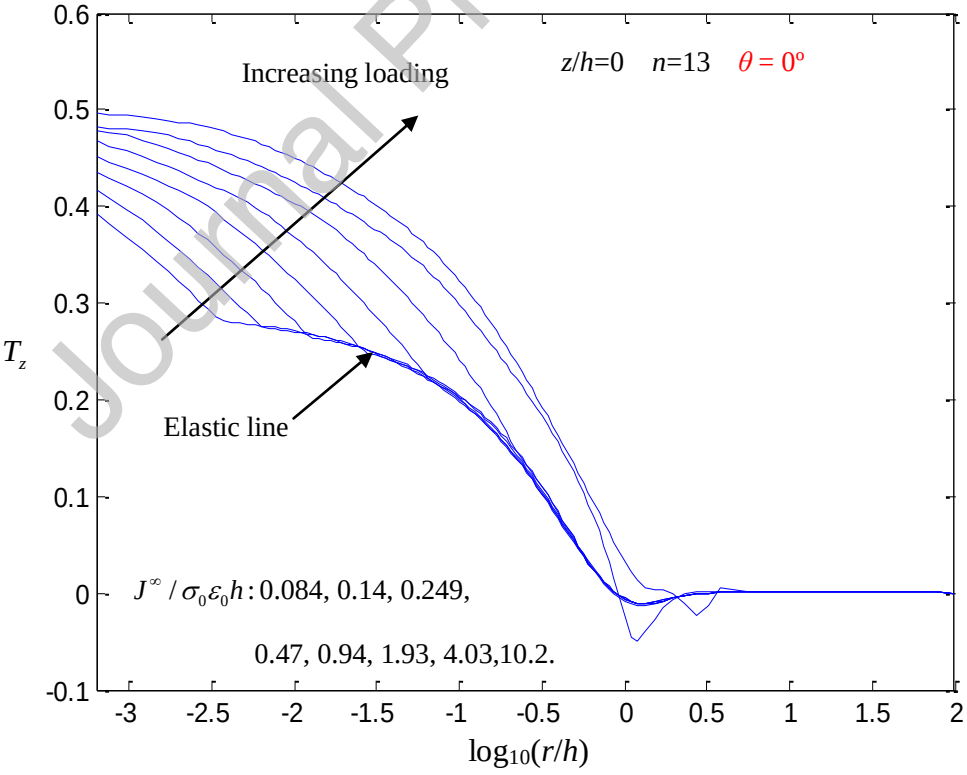
Increasing loading
z/h=0 n=13 θ = 0o
Elastic line
J∞ / σ0ε0h: 0.084, 0.14, 0.249,
0.47, 0.94, 1.93, 4.03,10.2.
Tz
log10(r/h)

(c)

Fig. 8

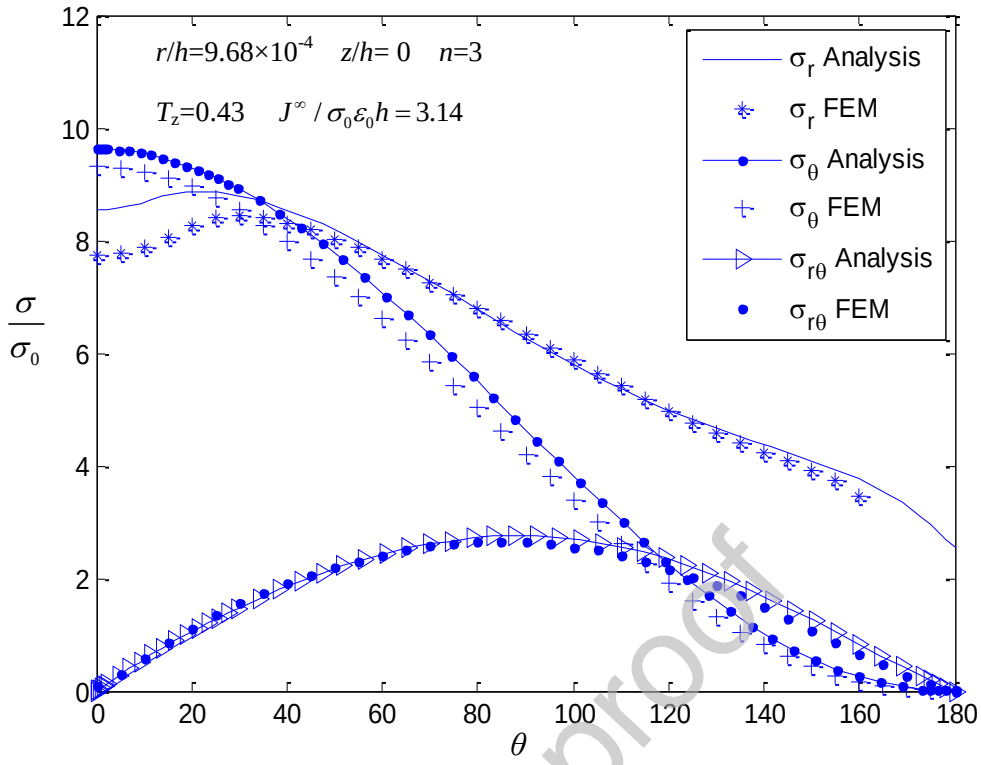

(a)

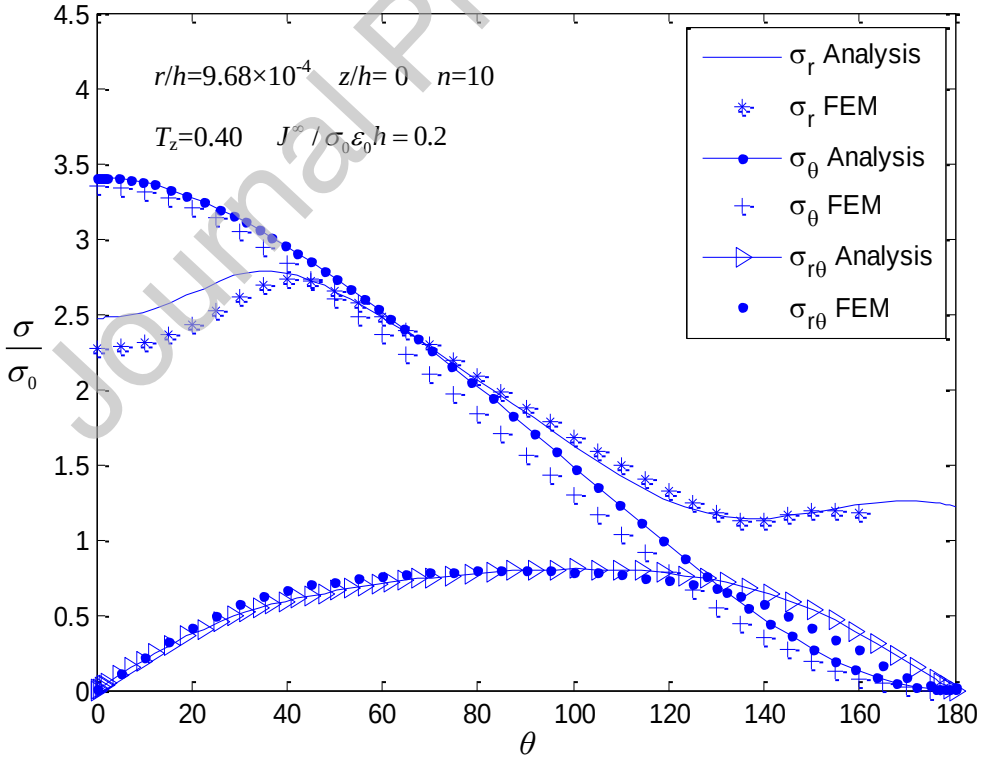

(b)

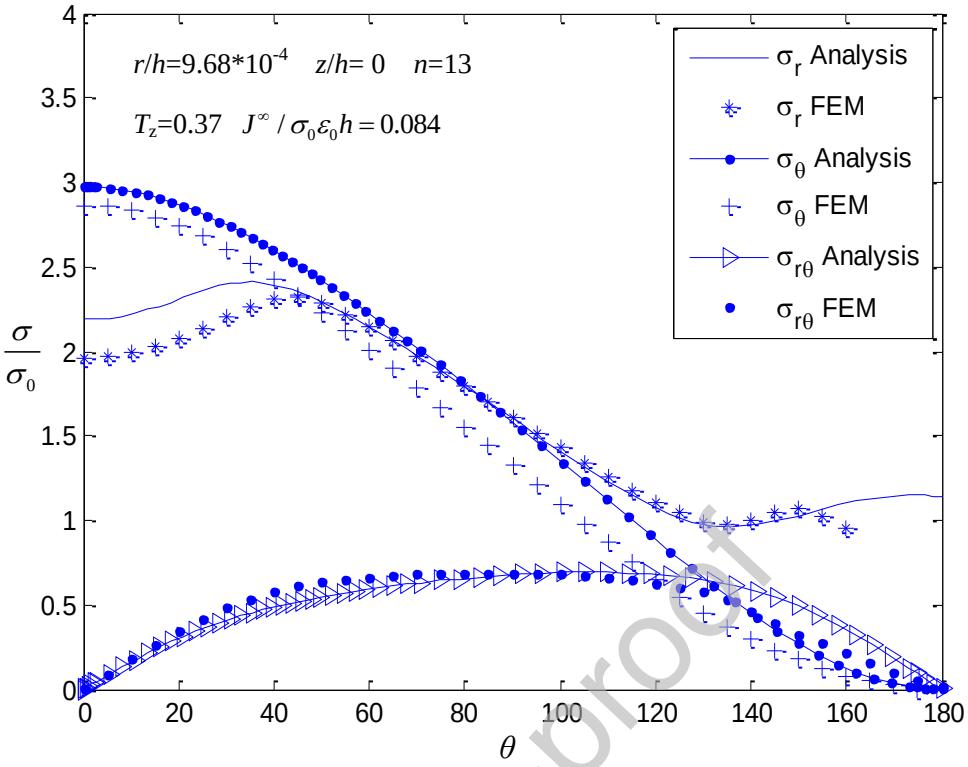

(c)

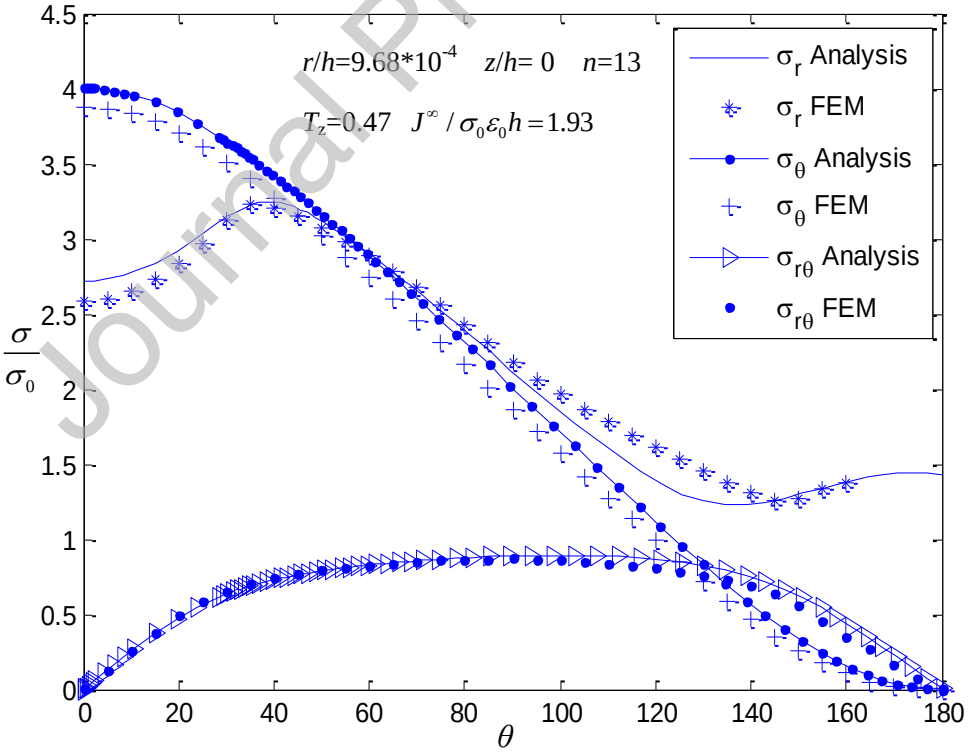

(d)

Fig. 9

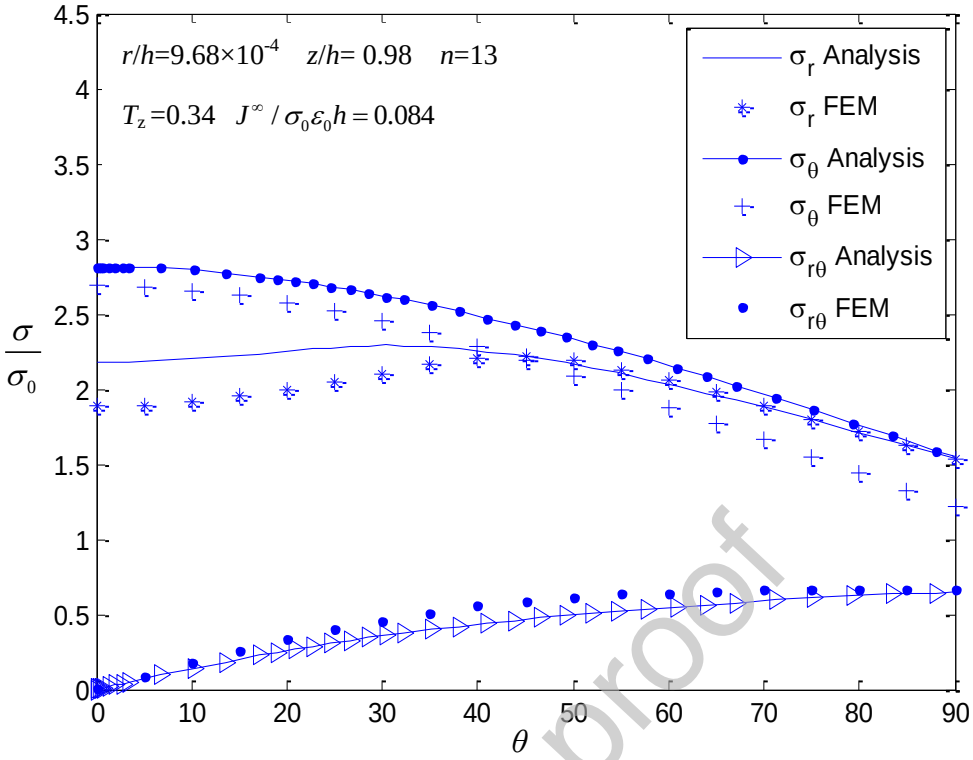

(a)

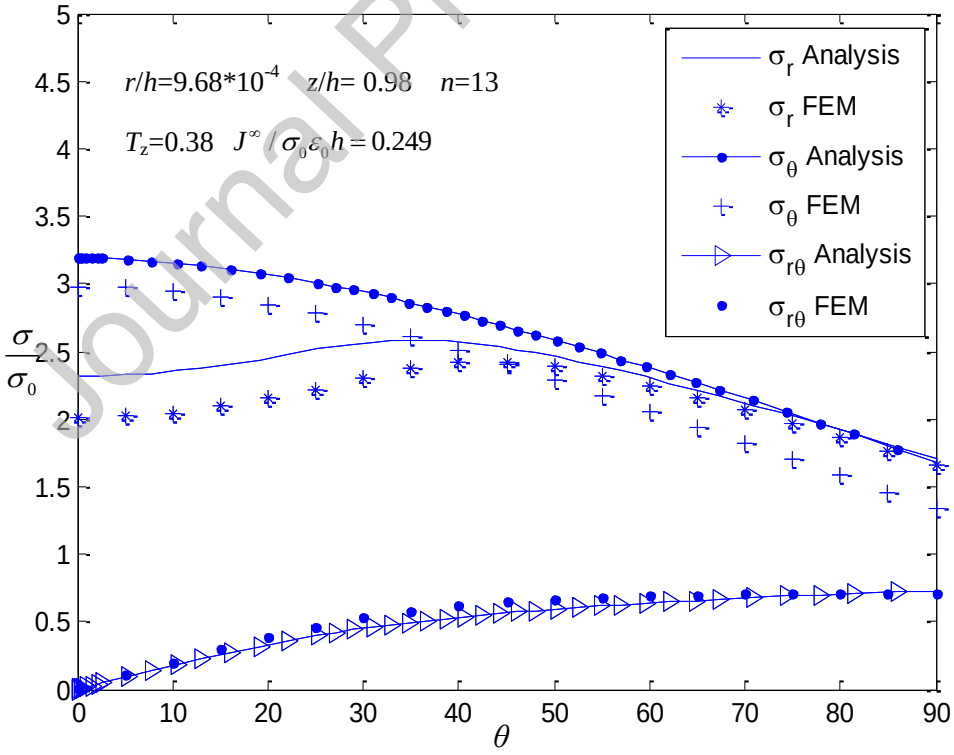

(b)

Fig. 10

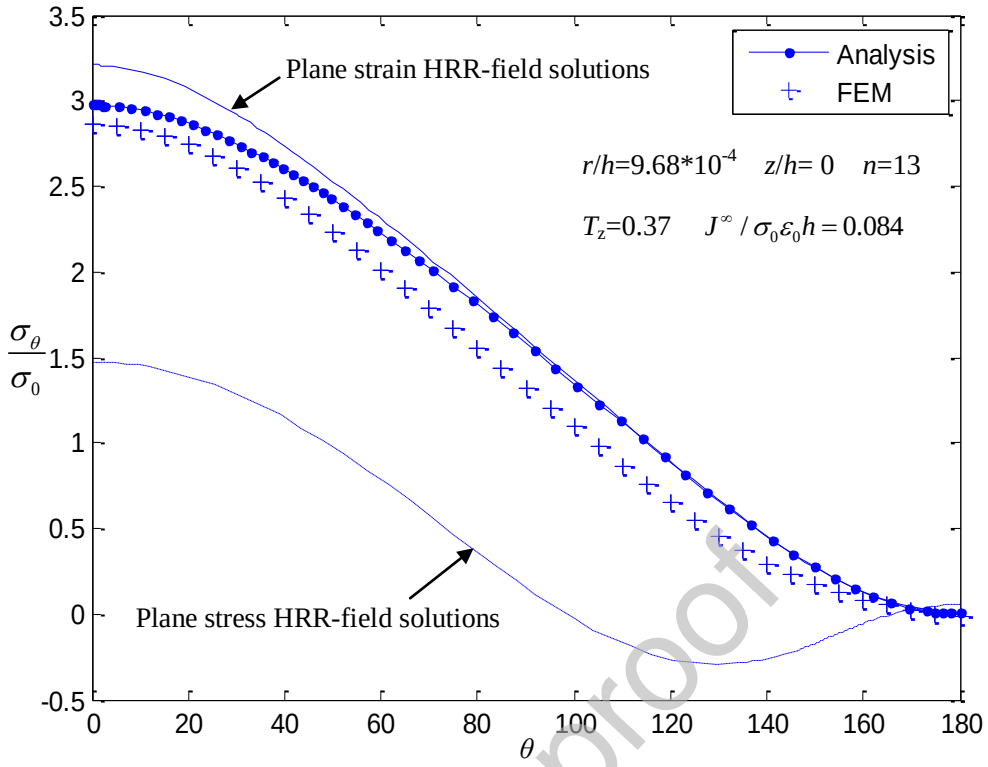

(a)

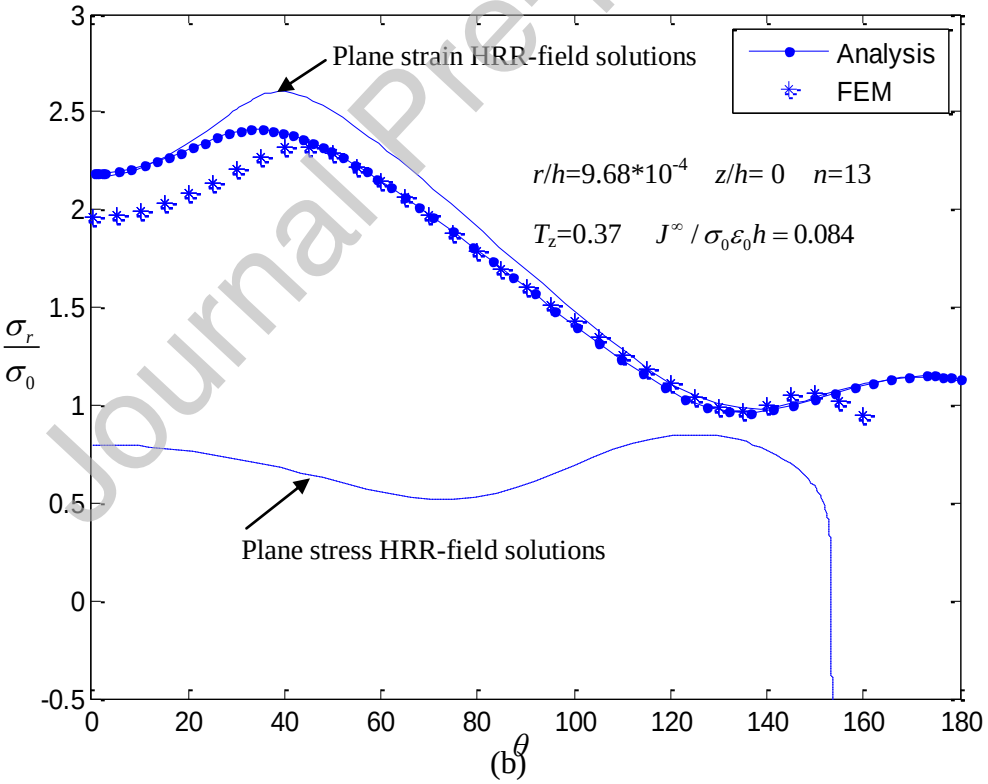

(b)

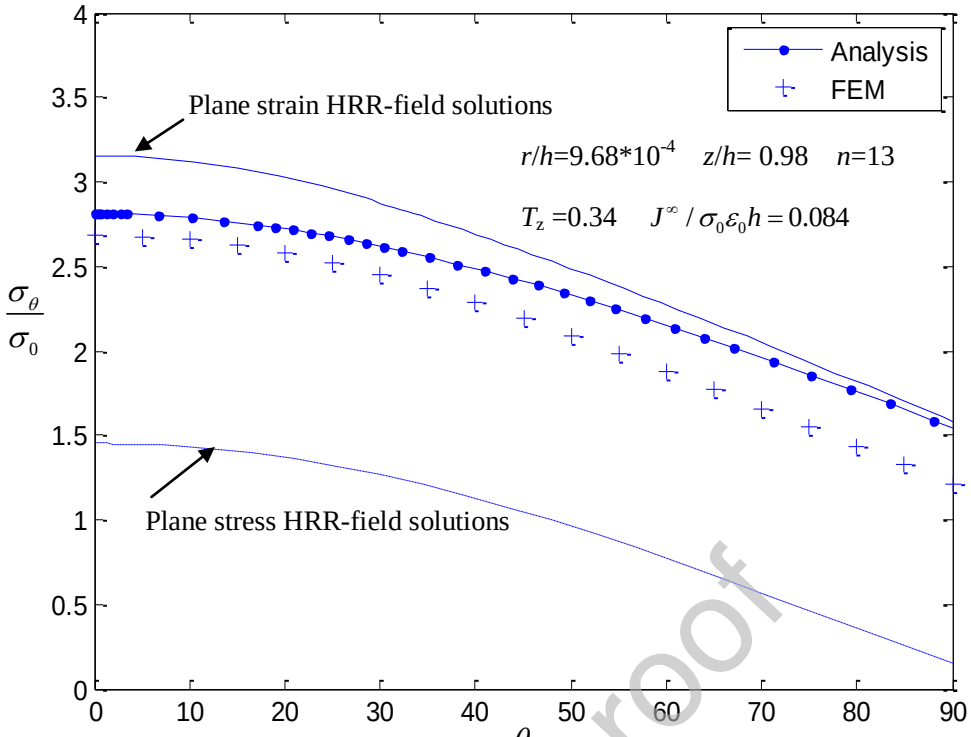

(c)

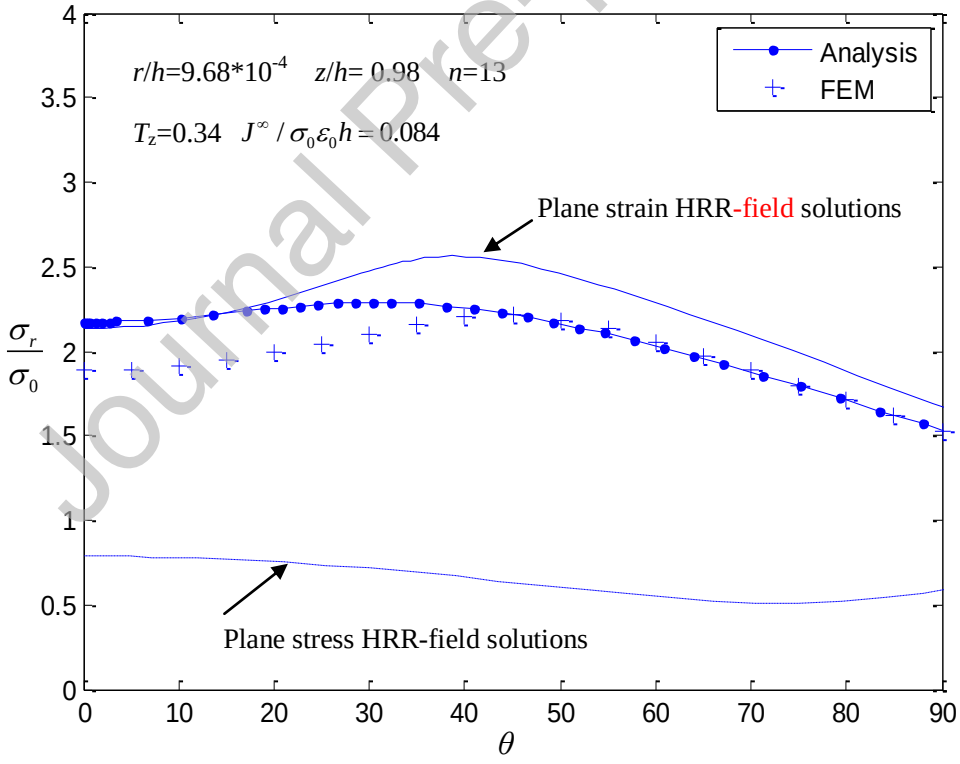

(d)

Fig.11

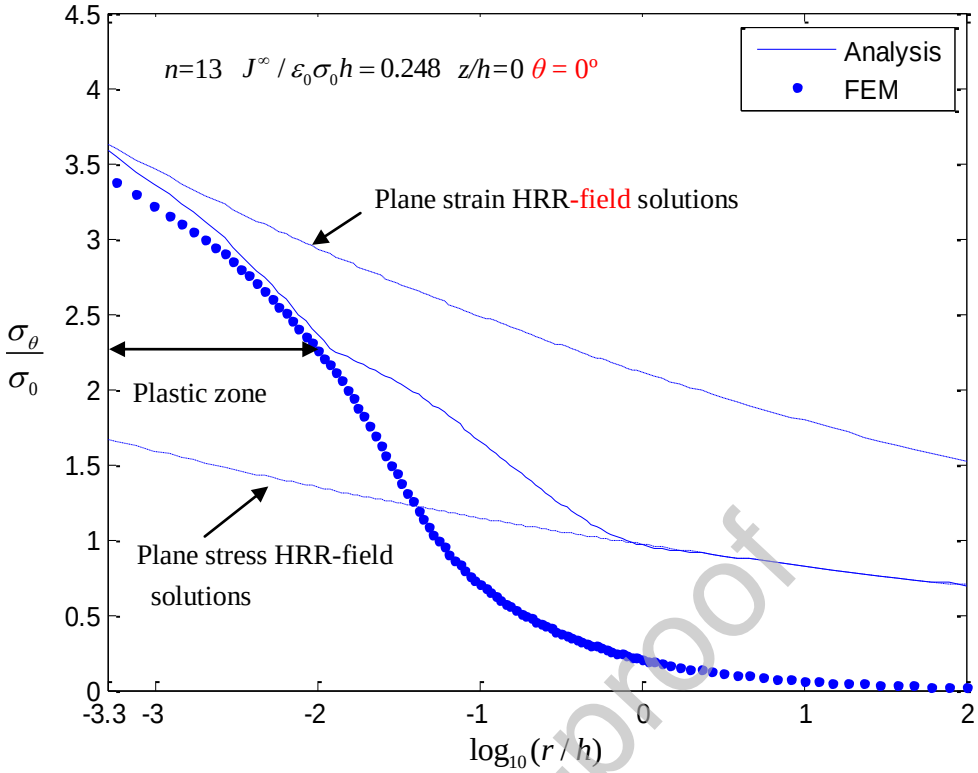

(a)

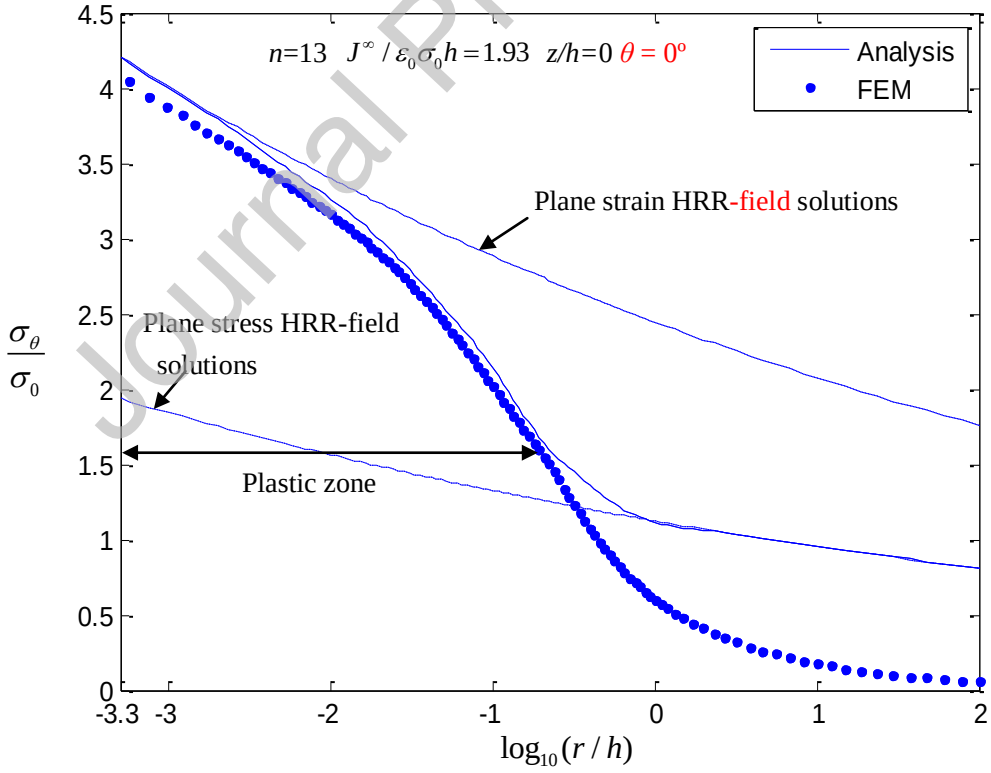

(b)

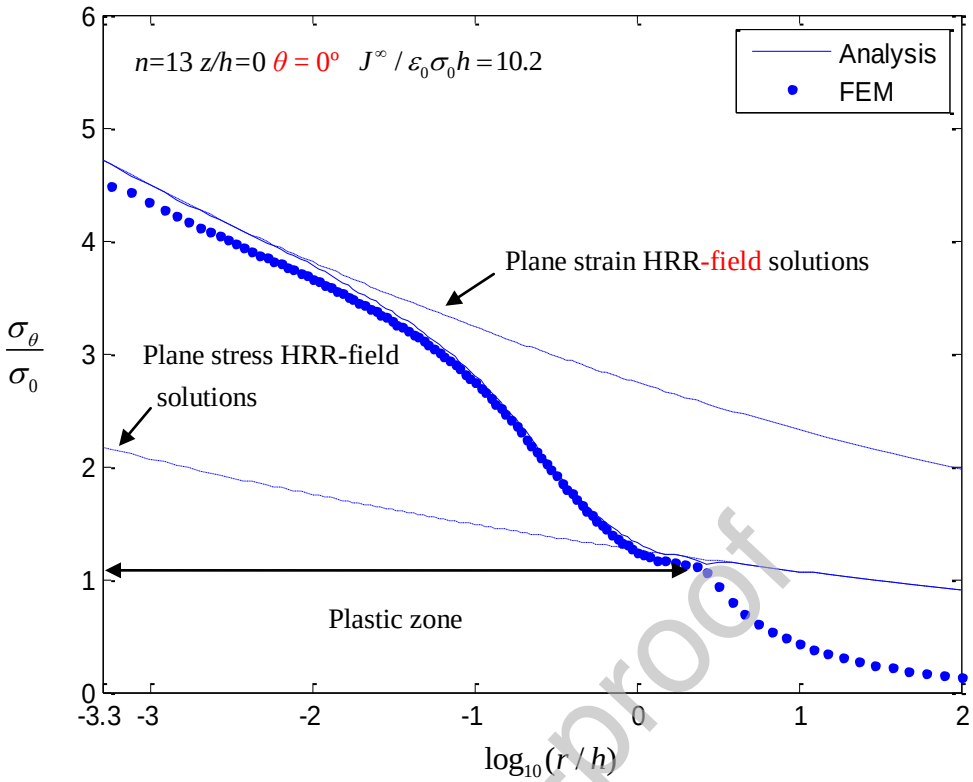

(c)

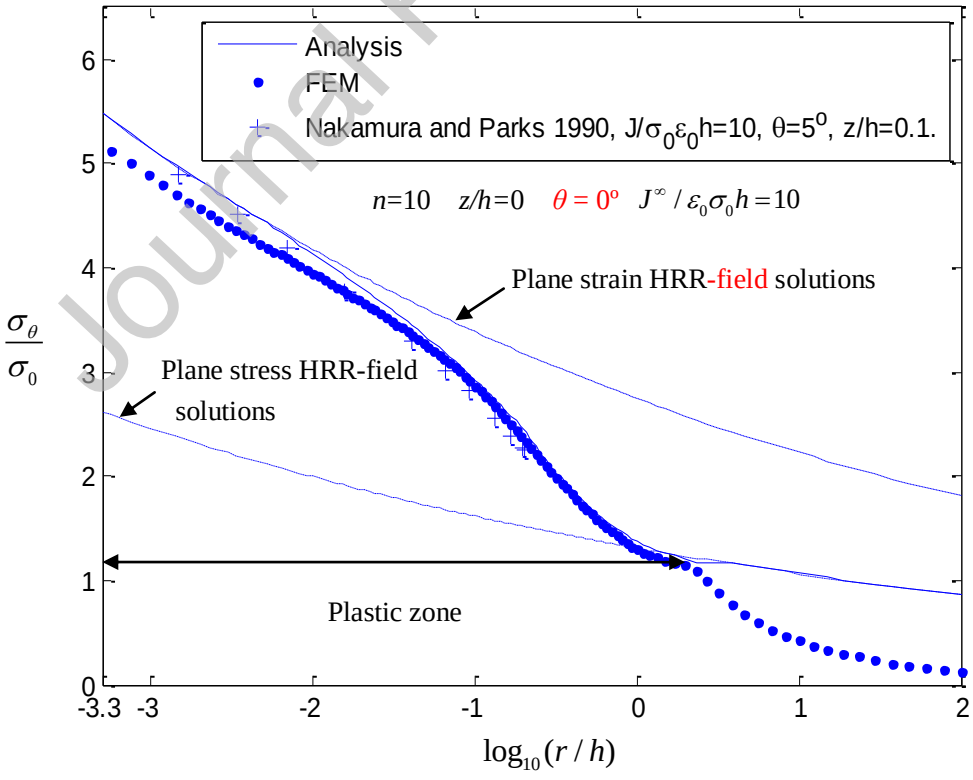

(d)

Table Caption

Table 1 Values of I with various T_z and n

T_z / I / n	0	0.05	0.1	0.15	0.2	0.25	0.3	0.35	0.4	0.45	0.5
3	3.86	4.14	4.46	4.80	5.12	5.38	5.46	5.39	5.36	5.43	5.51
10	2.95	3.26	3.59	4.05	4.57	4.87	4.17	4.18	4.28	4.43	4.52
13	2.87	3.14	3.51	3.96	4.40	4.70	4.00	4.01	4.14	4.29	4.40

Appendix A Expressions for $\tilde{u}_r$, $\tilde{u}_\theta$, $(\tilde{u}_r)^{\square}$, $(\tilde{u}_\theta)^{\square}$, H, $\tilde{A}$, $\tilde{B}$, $\tilde{C}$, $\tilde{D}$, $\tilde{E}$, $\tilde{F}$, $\left(\tilde{\sigma}_e^2\right)^{\square}$ and $\left(\tilde{\sigma}_e^2\right)^*$

Using the strain-displacement relation and the method of partial integration, the radial displacement u_r may be expressed by

$$u_r=\int \varepsilon_r dr=\frac{\alpha}{2E\sigma_0^{n-1}}\int K^n r^{(s-2)n}\tilde{\varepsilon}_r dr=\frac{\alpha}{2E\sigma_0^{n-1}\left(n(s-2)+1\right)}\int K^n\tilde{\varepsilon}_r d\left(r^{(s-2)n+1}\right)$$
$$=\frac{\alpha\left(K^n r^{(s-2)n+1}\tilde{\varepsilon}_r-\int r^{(s-2)n+1}\left(K^n\tilde{\varepsilon}_r\right)' dr\right)}{2E\sigma_0^{n-1}\left(n(s-2)+1\right)} \tag{A.1}$$

When r tends to zero, one may have

$$\lim_{r\to 0}\frac{\int r^{(s-2)n+1}\left(K^n\tilde{\varepsilon}_r\right)' dr}{K^n r^{(s-2)n+1}\tilde{\varepsilon}_r}=\frac{r^{(s-2)n+1}\left(K^n\tilde{\varepsilon}_r\right)'}{\left((s-2)n+1\right)K^n r^{(s-2)n}\tilde{\varepsilon}_r+r^{(s-2)n+1}\left(K^n\tilde{\varepsilon}_r\right)'}$$
$$=\frac{r\left(K^n\tilde{\varepsilon}_r\right)'}{\left((s-2)n+1\right)K^n\tilde{\varepsilon}_r+r\left(K^n\tilde{\varepsilon}_r\right)'}=0. \tag{A.2}$$

So, Eq. (A.1) may be re-written as

$$
\begin{aligned}
u_r &\approx \frac{\alpha K^n r^{(s-2)n+1}\tilde{\varepsilon}_r}{2E\sigma_0^{n-1}\left((s-2)n+1\right)} \\
&= \frac{\alpha K^n r^{(s-2)n+1}}{2E\sigma_0^{n-1}\left((s-2)n+1\right)}\tilde{\sigma}_e^{n-1}\left(\left(2-T_z\right)\left(s\tilde{\phi}+\tilde{\phi}'''\right)-\left(1+T_z\right)s(s-1)\tilde{\phi}'\right) \\
&= \frac{\alpha}{E\sigma_0^{n-1}}K^n r^{(s-2)n+1}\tilde{u}_r
\end{aligned}
\tag{A.3}
$$

$(u_r)'$, $(u_\theta)'$ and u_θ may be expressed as

$$
\left.
\begin{aligned}
(u_r)' &= \frac{\alpha}{E\sigma_0^{n-1}}K^n r^{(s-2)n+1}(\tilde{u}_r)' \\
&= \frac{\alpha K^n r^{(s-2)n+1}}{2E\sigma_0^{n-1}\left((s-2)n+1\right)}\left\{\left(\tilde{\sigma}_e^{n-1}\right)'\left(\left(2-T_z\right)\left(s\tilde{\phi}+\left(\tilde{\phi}\right)'''\right)-\left(1+T_z\right)s(s-1)\tilde{\phi}'\right)\right. \\
&\quad \left.+\tilde{\sigma}_e^{n-1}\left(\left(2-T_z\right)\left(s\left(\tilde{\phi}\right)'+\left(\tilde{\phi}\right)''''\right)-\left(1+T_z\right)s(s-1)\left(\tilde{\phi}\right)''\right)\right\}, \\
(u_\theta)' &= \varepsilon_\theta r - u_r = \frac{\alpha}{E\sigma_y^{n-1}}K^n r^{(s-2)n+1}(\tilde{u}_\theta)' \\
&= \frac{\alpha}{E\sigma_0^{n-1}}K^n r^{(s-2)n+1}\left(\frac{\tilde{\sigma}_e^{n-1}}{2}\left(\left(2-T_z\right)s(s-1)\tilde{\phi}-\left(1+T_z\right)\left(s\tilde{\phi}+\left(\tilde{\phi}\right)'''\right)\right)-\tilde{u}_r\right), \\
u_\theta &= \frac{\alpha}{E\sigma_0^{n-1}}K^n r^{(s-2)n+1}\tilde{u}_\theta = -\frac{\alpha}{E\sigma_0^{n-1}}K^n r^{(s-2)n+1}\frac{\left(3\tilde{\sigma}_e^{n-1}(s-1)\left(\tilde{\phi}\right)'+(\tilde{u}_r)'\right)}{n(s-2)}.
\end{aligned}
\right\}
\tag{A.4}
$$

$$
\begin{aligned}
H = &-\frac{3}{2}\tilde{B}(n-1)\left(\left(\frac{2\left(T_z\right)^2-2T_z-1}{3}s^2+s\right)\tilde{\phi}+\frac{2\left(\left(T_z\right)^2-T_z+1\right)}{3}\left(\tilde{\phi}'''\right)\right) \\
&-2\left(1+\left(T_z-1\right)T_z\right)\left(\tilde{\sigma}_e^2\right)
\end{aligned}
\tag{A.5}
$$

$$
\left.
\begin{aligned}
\tilde{A} &= \left(2s^2-3s\right)\tilde{\phi}-\tilde{\phi}'''+2\left(T_z-1\right)T_z\left(\tilde{\phi}'''+s^2\tilde{\phi}'\right), \\
\tilde{B} &= 2\tilde{\phi}'''+s(3-s)\tilde{\phi}+2\left(T_z-1\right)T_z\left(\tilde{\phi}'''+s^2\tilde{\phi}'\right), \\
\tilde{C} &= 6(s-1)\tilde{\phi}'', \\
\tilde{D} &= s\left(4s^2-9s+3\right)\tilde{\phi}+2(2s-3)\tilde{\phi}'''+2\left(T_z-1\right)T_z\left(2s-3\right)\left(s^2\tilde{\phi}'+\tilde{\phi}'''\right), \\
\tilde{E} &= 2\left(2s^2-3s+3\right)\tilde{\phi}''+4\tilde{\phi}''''+4\left(T_z-1\right)T_z\left(\tilde{\phi}''''+s^2\tilde{\phi}''\right), \\
\tilde{F} &= 2\left(1+\left(T_z-1\right)T_z\right)\left(s^2(s-2)^2\tilde{\phi}'+2\left(s^2-2s+2\right)\tilde{\phi}'''\right).
\end{aligned}
\right\}
\tag{A.6}
$$

$$\left(\tilde{\sigma}_e^2\right)^{\square}=3\left[\left(s(s-1)\tilde{\phi}-\frac{1+T_z}{3}\left(\tilde{\phi}^{\square}+s^2\tilde{\phi}\right)\right)\left(s(s-1)\left(\tilde{\phi}\right)^{\square}-\frac{1+T_z}{3}\left(\tilde{\phi}^{\square\square}+s^2\tilde{\phi}^{\square}\right)\right)\right.$$

$$+\left(s\tilde{\phi}+\tilde{\phi}^{\square}-\frac{1+T_z}{3}\left(\tilde{\phi}^{\square}+s^2\tilde{\phi}\right)\right)\left(s\tilde{\phi}^{\square}+\tilde{\phi}^{\square\square}-\frac{1+T_z}{3}\left(\tilde{\phi}^{\square\square}+s^2\tilde{\phi}^{\square}\right)\right)$$

$$\left.+\left(\frac{2T_z-1}{3}\right)^2\left(\tilde{\phi}^{\square}+s^2\tilde{\phi}\right)\left(\tilde{\phi}^{\square\square}+s^2\tilde{\phi}^{\square}\right)+2(1-s)^2\tilde{\phi}^{\square}\tilde{\phi}^{\square}\right] \tag{A.7}$$

and

$$\begin{aligned}\left(\tilde{\sigma}_e^2\right)^{*}=3\Bigg[&\left(s(s-1)\tilde{\phi}^{\square}-\frac{1+T_z}{3}\left(\tilde{\phi}^{\square\square}+s^2\tilde{\phi}^{\square}\right)\right)^2\\&+\left(s(s-1)\tilde{\phi}-\frac{1+T_z}{3}\left(\tilde{\phi}^{\square}+s^2\tilde{\phi}\right)\right)\left(s(s-1)-\frac{1+T_z}{3}s^2\right)\tilde{\phi}^{\square}\\&+\left(s\tilde{\phi}^{\square}+\tilde{\phi}^{\square\square}-\frac{1+T_z}{3}\left(\tilde{\phi}^{\square\square}+s^2\tilde{\phi}^{\square}\right)\right)^2\\&+\left(s\tilde{\phi}+\tilde{\phi}^{\square}-\frac{1+T_z}{3}\left(\tilde{\phi}^{\square}+s^2\tilde{\phi}\right)\right)\left(s-\frac{1+T_z}{3}s^2\right)\tilde{\phi}^{\square}\\&+\left(\frac{2T_z-1}{3}\right)^2\left(\tilde{\phi}^{\square\square}+s^2\tilde{\phi}^{\square}\right)^2+\left(\frac{2T_z-1}{3}\right)^2s^2\left(\tilde{\phi}^{\square}+s^2\tilde{\phi}\right)\tilde{\phi}^{\square}\\&+2(1-s)^2\left(\tilde{\phi}^{\square}\tilde{\phi}^{\square}+\tilde{\phi}^{\square}\tilde{\phi}^{\square\square}\right)\Bigg].\end{aligned} \tag{A.8}$$

Appendix B The derivation for Eq. (18)

Based on the principle of minimum complementary potential energy, one may have

$$\iiint_V\left(\varepsilon_x\delta\sigma_x+\varepsilon_y\delta\sigma_y+\varepsilon_z\delta\sigma_z+\gamma_{xy}\delta\sigma_{xy}+\gamma_{xz}\delta\sigma_{xz}+\gamma_{yz}\delta\sigma_{yz}\right)dxdydz=0\,. \tag{B.1}$$

Substituting Eq. (1) into Eq. (B.1), we have

$$\iiint_V\left[\varepsilon_x\delta\left(\frac{\partial^2\phi_2}{\partial z^2}+\frac{\partial^2\phi_3}{\partial y^2}\right)+\varepsilon_y\delta\left(\frac{\partial^2\phi_1}{\partial z^2}+\frac{\partial^2\phi_3}{\partial x^2}\right)+\varepsilon_z\delta\left(\frac{\partial^2\phi_1}{\partial y^2}+\frac{\partial^2\phi_2}{\partial x^2}\right)\right.$$

$$-\gamma_{xy}\frac{\partial^2\delta\phi_3}{\partial x\partial y}-\gamma_{xz}\frac{\partial^2\phi_2}{\partial x\partial z}-\gamma_{yz}\frac{\partial^2\phi_1}{\partial y\partial z}\Bigg]dxdydz=0 \tag{B.2}$$

.

According to derivation rules, one may have

$$\left.\begin{aligned}
\varepsilon_y\delta\left(\frac{\partial^2\phi_1}{\partial z^2}+\frac{\partial^2\phi_3}{\partial x^2}\right)&=\frac{\partial}{\partial z}\left(\varepsilon_y\frac{\partial(\delta\phi_1)}{\partial z}-\frac{\partial\varepsilon_y}{\partial z}\delta\phi_1\right)+\frac{\partial^2(\varepsilon_y)}{\partial z^2}\delta\phi_1+\frac{\partial}{\partial x}\left(\varepsilon_y\frac{\partial(\delta\phi_3)}{\partial x}-\frac{\partial\varepsilon_y}{\partial x}\delta\phi_3\right)\\
&\quad+\frac{\partial^2(\varepsilon_y)}{\partial x^2}\delta\phi_3,\\
\varepsilon_z\delta\left(\frac{\partial^2\phi_1}{\partial y^2}+\frac{\partial^2\phi_2}{\partial x^2}\right)&=\frac{\partial}{\partial y}\left(\varepsilon_z\frac{\partial(\delta\phi_1)}{\partial y}-\frac{\partial\varepsilon_z}{\partial y}\delta\phi_1\right)+\frac{\partial^2(\varepsilon_z)}{\partial y^2}\delta\phi_1+\frac{\partial}{\partial x}\left(\varepsilon_z\frac{\partial(\delta\phi_2)}{\partial x}-\frac{\partial\varepsilon_z}{\partial x}\delta\phi_2\right)\\
&\quad+\frac{\partial^2(\varepsilon_z)}{\partial x^2}\delta\phi_2,\\
-\gamma_{xy}\frac{\partial^2(\delta\phi_3)}{\partial x\partial y}&=-\frac{\partial\left(\gamma_{xy}\frac{\partial}{\partial y}\delta\phi_3\right)}{\partial x}+\frac{\partial}{\partial y}\left(\frac{\partial\gamma_{xy}}{\partial x}\delta\phi_3\right)-\frac{\partial^2(\gamma_{xy})}{\partial y\partial x}\delta\phi_3,\\
-\gamma_{xz}\frac{\partial^2(\phi_2)}{\partial x\partial z}&=-\frac{\partial\left(\gamma_{xz}\frac{\partial}{\partial z}\delta\phi_2\right)}{\partial x}+\frac{\partial}{\partial z}\left(\frac{\partial\gamma_{xz}}{\partial x}\delta\phi_2\right)-\frac{\partial^2(\gamma_{xz})}{\partial z\partial x}\delta\phi_2,\\
-\gamma_{yz}\frac{\partial^2(\phi_1)}{\partial y\partial z}&=-\frac{\partial\left(\gamma_{yz}\frac{\partial}{\partial z}\delta\phi_1\right)}{\partial y}+\frac{\partial}{\partial z}\left(\frac{\partial\gamma_{yz}}{\partial y}\delta\phi_1\right)-\frac{\partial^2(\gamma_{yz})}{\partial z\partial y}\delta\phi_1.
\end{aligned}\right\} \tag{B.3}$$

Substituting Eq. (B.3) into Eq. (B.2), Eq. (B.3) may be re-written as

$$\iiint_V \frac{\partial}{\partial x}\left(-\frac{\partial \varepsilon_z}{\partial x}\delta\phi_2-\frac{\partial \varepsilon_y}{\partial x}\delta\phi_3+\varepsilon_z\frac{\partial(\delta\phi_2)}{\partial x}-\gamma_{xz}\frac{\partial(\delta\phi_2)}{\partial z}+\varepsilon_y\frac{\partial(\delta\phi_3)}{\partial x}-\gamma_{xy}\frac{\partial(\delta\phi_3)}{\partial y}\right)dxdydz$$
$$+\iiint_V \frac{\partial}{\partial y}\left(-\frac{\partial \varepsilon_z}{\partial y}\delta\phi_1+\left(\frac{\partial \gamma_{xy}}{\partial x}-\frac{\partial \varepsilon_x}{\partial y}\right)\delta\phi_3+\varepsilon_z\frac{\partial(\delta\phi_1)}{\partial y}-\gamma_{yz}\frac{\partial(\delta\phi_1)}{\partial z}+\varepsilon_x\frac{\partial(\delta\phi_3)}{\partial y}\right)dxdydz$$
$$+\iiint_V \frac{\partial}{\partial z}\left(\left(\frac{\partial \gamma_{yz}}{\partial y}-\frac{\partial \varepsilon_y}{\partial z}\right)\delta\phi_1+\left(\frac{\partial \gamma_{xz}}{\partial x}-\frac{\partial \varepsilon_x}{\partial z}\right)\delta\phi_2+\varepsilon_y\frac{\partial(\delta\phi_1)}{\partial z}+\varepsilon_x\frac{\partial(\delta\phi_2)}{\partial z}\right)dxdydz$$
$$+\iiint_V \left[\left(\frac{\partial^2(\varepsilon_z)}{\partial y^2}+\frac{\partial^2(\varepsilon_y)}{\partial z^2}-\frac{\partial^2\gamma_{yz}}{\partial z\partial y}\right)\delta\phi_1+\left(\frac{\partial^2(\varepsilon_z)}{\partial x^2}+\frac{\partial^2(\varepsilon_x)}{\partial z^2}-\frac{\partial^2\gamma_{xz}}{\partial z\partial x}\right)\delta\phi_2\right.$$
$$\left.+\left(\frac{\partial^2(\varepsilon_y)}{\partial x^2}+\frac{\partial^2(\varepsilon_x)}{\partial y^2}-\frac{\partial^2\gamma_{xy}}{\partial y\partial x}\right)\delta\phi_3\right]dxdydz=0 \tag{B.4}$$

Further, Eq. (B.4) may be re-written as

$$\iint_{S_1}\left(-\frac{\partial \varepsilon_z}{\partial x}\delta\phi_2-\frac{\partial \varepsilon_y}{\partial x}\delta\phi_3+\varepsilon_z\frac{\partial(\delta\phi_2)}{\partial x}-\gamma_{xz}\frac{\partial(\delta\phi_2)}{\partial z}+\varepsilon_y\frac{\partial(\delta\phi_3)}{\partial x}-\gamma_{xy}\frac{\partial(\delta\phi_3)}{\partial y}\right)dydz$$
$$+\iint_{S_2}\left(-\frac{\partial \varepsilon_z}{\partial y}\delta\phi_1+\left(\frac{\partial \gamma_{xy}}{\partial x}-\frac{\partial \varepsilon_x}{\partial y}\right)\delta\phi_3+\varepsilon_z\frac{\partial(\delta\phi_1)}{\partial y}-\gamma_{yz}\frac{\partial(\delta\phi_1)}{\partial z}+\varepsilon_x\frac{\partial(\delta\phi_3)}{\partial y}\right)dxdz$$
$$+\iint_{S_3}\left(\frac{\partial \gamma_{yz}}{\partial y}-\frac{\partial \varepsilon_y}{\partial z}\right)\delta\phi_1+\left(\frac{\partial \gamma_{xz}}{\partial x}-\frac{\partial \varepsilon_x}{\partial z}\right)\delta\phi_2+\varepsilon_y\frac{\partial(\delta\phi_1)}{\partial z}+\varepsilon_x\frac{\partial(\delta\phi_2)}{\partial z}dxdy$$
$$\iiint_V \left[\left(\frac{\partial^2(\varepsilon_z)}{\partial y^2}+\frac{\partial^2(\varepsilon_y)}{\partial z^2}-\frac{\partial^2(\gamma_{yz})}{\partial z\partial y}\right)\delta\phi_1+\left(\frac{\partial^2(\varepsilon_z)}{\partial x^2}+\frac{\partial^2(\varepsilon_x)}{\partial z^2}-\frac{\partial^2(\gamma_{xz})}{\partial z\partial x}\right)\delta\phi_2\right.$$
$$\left.+\left(\frac{\partial^2(\varepsilon_y)}{\partial x^2}+\frac{\partial^2(\varepsilon_x)}{\partial y^2}-\frac{\partial^2(\gamma_{xy})}{\partial y\partial x}\right)\delta\phi_3\right]dxdydz=0 \tag{B.5}$$

Noting compatibility equations, the last integral in Eq. (B.5) should be zero. Furthermore, noting $\phi_1=\phi_2=T_z\phi_3$, the last integral in Eq. (B.5) can be re-written as

$$\iiint_V \left[T_z\left(\frac{\partial^2(\varepsilon_z)}{\partial x^2}+\frac{\partial^2(\varepsilon_z)}{\partial y^2}-\frac{\partial^2(\gamma_{xz})}{\partial z\partial x}-\frac{\partial^2(\gamma_{yz})}{\partial z\partial y}+\frac{\partial^2(\varepsilon_x)}{\partial z^2}+\frac{\partial^2(\varepsilon_y)}{\partial z^2}\right)\right.$$
$$\left.+\left(\frac{\partial^2(\varepsilon_y)}{\partial x^2}+\frac{\partial^2(\varepsilon_x)}{\partial y^2}-\frac{\partial^2(\gamma_{xy})}{\partial y\partial x}\right)\right]\delta\phi_3 dxdydz=0 \tag{B.6}$$

When r tends to zero, Eq.(B.6) may be re-written as

$$\iiint_V \left[T_z \left(\frac{\partial^2(\varepsilon_z)}{\partial x^2} + \frac{\partial^2(\varepsilon_z)}{\partial y^2} - \frac{\partial^2(\gamma_{xz})}{\partial z \partial x} - \frac{\partial^2(\gamma_{yz})}{\partial z \partial y} + \frac{\partial^2(\varepsilon_x)}{\partial z^2} + \frac{\partial^2(\varepsilon_y)}{\partial z^2} \right) + \left(\frac{\partial^2(\varepsilon_y)}{\partial x^2} + \frac{\partial^2(\varepsilon_x)}{\partial y^2} - \frac{\partial^2(\gamma_{xy})}{\partial y \partial x} \right) \right] \delta\phi_3 dxdydz \tag{B.7}$$

$$\approx \iiint_V \left[T_z \left(\frac{\partial^2(\varepsilon_z)}{\partial x^2} + \frac{\partial^2(\varepsilon_z)}{\partial y^2} \right) + \left(\frac{\partial^2(\varepsilon_y)}{\partial x^2} + \frac{\partial^2(\varepsilon_x)}{\partial y^2} - \frac{\partial^2(\gamma_{xy})}{\partial y \partial x} \right) \right] \delta\phi_3 dxdydz$$

$\delta\phi_3$ is arbitrary, one has

$$T_z \left(\frac{\partial^2(\varepsilon_z)}{\partial x^2} + \frac{\partial^2(\varepsilon_z)}{\partial y^2} \right) + \left(\frac{\partial^2(\varepsilon_y)}{\partial x^2} + \frac{\partial^2(\varepsilon_x)}{\partial y^2} - \frac{\partial^2(\gamma_{xy})}{\partial y \partial x} \right) = 0. \tag{B.8}$$

Eq. (B.8) may be re-written as in a cylindrical coordinate system

$$\left((r\varepsilon_\theta)'' + \frac{(\varepsilon_r)''}{r} - (\varepsilon_r)' - (\gamma_{r\theta})'' - \left(\frac{\gamma_{r\theta}}{r} \right)' \right) + T_z \left(\frac{1}{r}(\varepsilon_z)'' + (\varepsilon_z r)'' - (\varepsilon_z)' \right) = 0.$$